Journal of Power Sources 456 (2020) 227984

Contents lists available at ScienceDirect

Journal of Power Sources

journal homepage: www.elsevier.com/locate/jpowsour

Enhanced online model identification and state of charge estimation for lithium-ion battery under noise corrupted measurements by bias compensation recursive least squares

Yigang Li [a,b], Jiqing Chen [a,b], Fengchong Lan [a,b,*]

[a] School of Mechanical & Automotive Engineering, South China University of Technology, Guangzhou, 510641, China
[b] Guangdong Key Laboratory of Automotive Engineering, Guangzhou, 510641, China

HIGHLIGHTS

- Noise corruption on battery model identification bias in RLS is investigated.
- Biases generated even only voltage or current measurement is corrupted by noise.
- Noise effect on conventional RLS based co-estimation algorithm is investigated.
- Three bias compensation RLS based co-estimation algorithms are proposed.
- The superiority of the proposed methods is verified by simulations and experiments.

ARTICLE INFO

Keywords:
Model identification
Recursive least squares
Noise
State of charge
Co-estimation
Bias compensation

ABSTRACT

In online battery model identification by recursive least squares (RLS), the identification biases are generated by the noises in the voltage and current measurements, further resulting in the accuracy degradation of model-based state of charge (SOC) estimation. Firstly, the detailed formula derivation presents the relationship between noise variances and identification biases in least squares. Then, through the practical identification on a general battery model, the consistent results from the formulas and simulations both adequately and quantitatively verify that the model identified by RLS is biased, when either only one of voltage and current measurements or both are corrupted by noises. To further assess the noise effects on SOC and parameter estimations, a conventional co-estimation algorithm joining RLS and extended Kalman filter (EKF) is applied into the simulations and experiments especially under noise corrupted measurements, the numerical results show that the estimation accuracy degradation generated by noises is quite considerable. Hence, bias compensation RLS and EKF co-estimation algorithms are proposed to alleviate the impact of the noises. Simulation and experiment studies show that the proposed algorithms can compensate the model identification biases caused by noises and can enhance SOC estimation accuracy under noise corrupted measurements.

1. Introduction

Due to the advantages of high power rating, high energy density and long cycle life, lithium-ion batteries have been widely used in energy storage systems and electrical vehicles. In order to improve safety, reliability, efficiency, and longevity of battery system, a battery management system (BMS) needs to be well designed for monitoring essential states of battery systems. Accurately and reliably monitoring battery state of charge (SOC) is one of main requirements of BMS. So far, there are mainly four groups of SOC estimation methods, namely look-up table based methods, Ampere-hour integral methods, data-driven estimation methods, and model-based estimation methods [1]. A look-up table based method infers SOC from the relationships between SOC and one or more parameters, such as open circuit voltage (OCV) or impedance [2–4]. The precise measurement of OCV requires the battery rest for sufficient time after ending current interruption, so looking-up the table between SOC and OCV cannot acquire SOC in real-time. The measurement of battery impedance needs additional measurement

* Corresponding author. Room 1301, Building of Automotive Engineering Institute, No.381, Wushan Road, Tianhe District, Guangzhou City, Guangdong Province, China.
E-mail addresses: lygcsu06@126.com (Y. Li), chjq@scut.edu.cn (J. Chen), lfc1301@hotmail.com, fclan@scut.edu.cn (F. Lan).

https://doi.org/10.1016/j.jpowsour.2020.227984
Received 31 August 2019; Received in revised form 21 January 2020; Accepted 29 February 2020
Available online 13 March 2020
0378-7753/

equipment, thus, looking-up the table between SOC and impedance is not suitable for running EVs. An ampere-hour integral method is easy to implement, but suffers from uncertainty in initial state, measurement errors of battery current, and error accumulation over time [1]. A data-driven estimation method does not require an accurate battery model, but suffers from highly dependent on training data and high computation complexity [5–10].

Another widely used group of SOC estimation methods is model-based method with the good robustness performance due to their closed-loop feedback mechanism [11]. A variety of state estimation algorithms and adaptive filters are applied to estimate the SOC of batteries, such as Kalman filter [12–20], particle filter [21–23], Luenberger observer [24], H-infinity filter [25–27], and sliding-mode observer [28,29] et al. The Battery model is needed in model-based estimation method. The battery model can be identified by offline or online methods. In offline identification method, the battery model cannot change in real-time. However, battery model parameters have to change in working with a lot of factors, such as temperature, SOC, and battery ageing [30–32]. The inaccuracy in battery model unavoidably reduces the estimation accuracy of SOC, and even causes filter divergence. For this reason, the online identification battery model in model-based estimation method should be carefully addressed. The online identification of battery model is not only required for SOC estimation, but also useful for system diagnosis and efficiency enhancement [30,33].

One group of model parameter and SOC co-estimation methods are joint/dual estimations. In a joint estimation, the parameters of model are augmented to the state vector. The augmented state vector is estimated by various filters or observers. A dual estimation method uses two separate adaptive filters, instead of only one, to simultaneously estimate parameters and states, one for SOC estimation and the other one for model parameter estimation. The joint extended Kalman filter (EKF) in Ref. [16,34], the joint unscented Kalman filter in Refs. [35,36], the dual EKF in Refs. [16], and the dual sigma point Kalman filter in Refs. [35,37] were employed for simultaneous state and parameter estimation. In Ref. [38,39], the multiscale framework with dual EKF was employed.

The other group of model parameter and SOC co-estimation methods realize online model identification by recursive least squares (RLS) or moving window least-squares, while the SOC estimated by a variety of state estimation methods. Xiong et al. [40] used RLS for online model parameter identification, while SOC estimation was realized by an adaptive extended Kalman filter. Guo et al. [41] used RLS for online model parameter identification, while SOC estimation was realized by an adaptive unscented Kalman filter. Li et al. [42] proposed a novel combination algorithm of strong tracking unscented Kalman filter and adaptive unscented Kalman filter to estimate SOC, while the model parameter was achieved by a RLS method with fuzzy adaptive forgetting factor. In the study of Rahimi-Eichi [43], the moving window least squares was implemented to online identify the battery model, while the SOC was estimated by an observer. Xia et al. [44] co-estimated parameter and SOC in variable temperature by forgetting factor RLS and nonlinear Kalman filter. Lao et al. [45] co-estimated parameter and SOC in variable temperature by variable forgetting factor RLS and unscented Kalman filter.

In practical application, both voltage and current measurements in BMS are inevitably corrupted by noise. This is the errors in variables (EIV) problems in system identification [46], in which both output and input measurements of the system are corrupted by noises. As shown in Ref. [46–48] the conventional RLS identification method gives biased parameter estimation for the EIV problem. Inaccurate model parameters will reduce the estimation accuracy for model-based SOC estimation algorithms [44,45,49], so biased parameter estimation not only reduces the accuracy of parameter identification, but also reduces the SOC estimation accuracy in model-based SOC estimations. Some works have addressed the noise effect in BMS. Sitterly et al. [50] corrected the identification biases on battery model parameters in RLS by assuming the noise characteristics were known. Liu et al. [51] reduced noise effects by signal averaging. The signals have to be sampled at a much faster rate than the SOC estimation. This needs faster sampler and consumes more amount of memory. Wei et al. proposed a parameter and SOC co-estimation algorithm for lithium-ion battery by using a Frisch scheme based bias compensating RLS to compensate the noise effect in [30]. Wei et al. later proposed a recursive total least squares based observer for co-estimation parameter and SOC of lithium-ion battery in [52] to alleviate the noise effect. In Ref. [53], Wei et al. integrated recursive total least squares with EKF to address the noise effect in parameter and SOC co-estimation of lithium-ion battery. The bias compensation method used in Ref. [30,52,53] are all for EIV problem, in which the effect of the noises on both voltage and current measurements are considered, but the cases, when only voltage or current measurement is corrupted by noise, is not investigated. It is notable that when the variance of noise on input measurement is zero or negligible, the EIV problem turns into output error (OE) problem. As shown in Ref. [48,54], in OE problem, the conventional RLS identification method still gives biased estimation. Similarly, when the variance of noise on output measurement is zero or negligible, the EIV problem turns into input error (IE) problem. Comparing with EIV problem, one of the advantages of solving OE and IE problems is that only the variance of noise on output or input measurement, instead of noises on output and input measurements, is needed to compensate the estimation biases. It indicates that the algorithms to compensate bias for OE and IE problems potentially need less computation cost and have better numerical stability compared to that for the EIV problem. When the variance of noise on input or output measurement is negligible, bias compensation for OE and IE problem potentially more suitable in online identification with less computation cost and better numerical stability. According to the analyses on OE and IE problems, even only one of voltage and current measurements is corrupted by noise, the noise still leads to bias of battery model identified by RLS and further reduces the SOC estimation accuracy in model-based SOC estimation. This will be verified in this research by formula derivations and simulation studies.

In this paper, in order to address the battery model identification biases caused by noises in the widely used RLS method, and the adverse effect on model-based SOC estimation, three noise corruption problems in BMS are investigated. The first one is the EIV problem, in which both the output (voltage) and input (current) measurements are corrupted by noises. The second and the third one are OE problem and IE problem, in which only the output (voltage) measurement or the input (current) measurement is corrupted by noise. Firstly, in order to clearly understand the identification biases caused by noises in the conventional RLS, the detailed formula derivation which presents the relationship between noise variances and identification biases in least squares (LS) is carried out. Then, the widely used first-order RC model is selected as a study object, the influence of the noises on identification biases in this model by conventional RLS is investigated by experimental simulations. The consistent results from bias formulas and simulations both adequately and quantitatively verify that the battery model identified by conventional RLS is biased not only when both voltage and current measurements are corrupted by noises, but also when only one of them is corrupted by noise. In order to assess adverse noise effect on the conventional RLS-based parameter and SOC co-estimation methods, the influences of the noise on SOC and parameter identification in conventional joint forgetting factor recursive least squares (FRLS) and EKF co-estimation algorithm (FRLS-EKF) is investigated by simulations and experiments. The results show that noises result in biases in battery model identification and greatly deteriorate the estimation of SOC in all three noise corruption problems. To alleviate the noise effect, three joint bias compensation RLS and EKF co-estimation algorithms are proposed for different noise corruption problems. The first one is based on forgetting factor bias compensation RLS for OE problem (FBCRLSOE), which can compensate the identification biases caused by the noise, when only voltage measurement is corrupted by noise. The second one is based on forgetting factor bias compensation RLS for IE problem

(FBCRLSIE), which can compensate the identification biases caused by the noise, when only current measurement is corrupted by noise. The third one is based on forgetting factor bias compensation RLS for EIV problem (FBCRLSEIV), which can compensate the identification biases caused by noises imposed on both voltage and current measurements. The simulation and experiment studies are conducted to assess the performances of the proposed algorithms, comparing with conventional FRLS-EKF, the proposed bias compensation RLS based co-estimation algorithms can effectively compensate the model identification biases caused by noises and enhance SOC estimation accuracy under the noise corrupted measurements. Moreover, in order to evaluate the feasibility of the proposed algorithm in online application, the computation costs of these algorithms are evaluated by counting the arithmetic operation requirements of each algorithm. As a result, the proposed bias compensation RLS-based co-estimation algorithm can be used in online application with moderate growth in computation cost.

The rest of this paper is organized as follows: in Section 2, the first-order RC model of lithium-ion battery is detailed, the offline model identification by genetic algorithm is also presented; in Section 3, the identification biases in least squares under noise corruption is investigated by detailed formula derivation and simulation; in Section 4, the joint algorithm of bias compensation RLS and EKF are proposed; in Section 5 and Section 6, the performances of the joint algorithm based on conventional RLS and the joint algorithms based on bias compensation RLS are compared by simulations and experiments, respectively; Section 7 concludes this paper.

2. Previous preparation

2.1. Experiment setup

A Samsung 18650 lithium-ion battery with nominal capacity of 2900 mAh is used as the experiment subject, with specifications of the nominal voltage 3.6 V, discharging end voltage 2.5 V and charging end voltage 4.2 V. The experiment setup is shown schematically in Fig. 1 (a). The current profile is executed on a Neware BTS-4008 battery test system with current and voltage ranges of −6–6 A and 0 ~ 5V, respectively. The measurement accuracy is within 0.1% for both. The experiment data

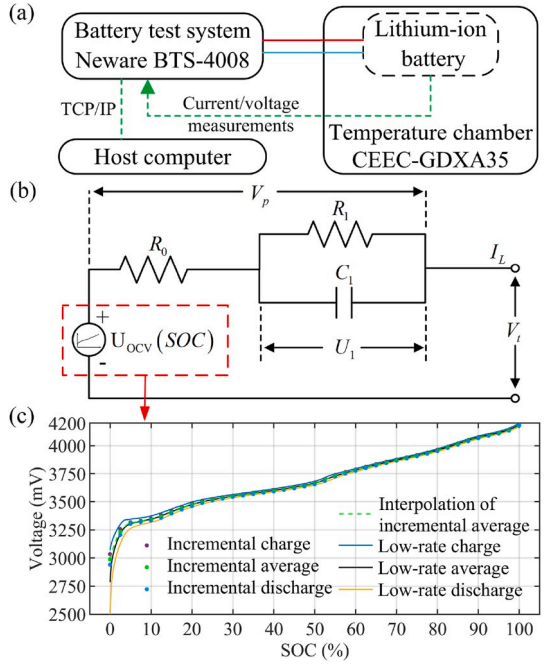

Fig. 1. (a) Schematic of experiment setup; (b) schematic diagram of first-order RC battery model; (c) OCV-SOC test results.

are collected by the battery test system with the sampling time interval of 1 s. A programmable temperature chamber (error within ±1 °C) is used to control the test temperature.

2.2. Battery modeling and OCV-SOC test

There are mainly three categories of battery models: electrochemical model (EM), equivalent circuit model (ECM) and electrochemical impedance model (EIM) [1]. In the practical application, ECMs are widely used in model-based SOC estimation. Several kinds of ECMs have been proposed by now [55–58]. Considering complexity and precision, the first-order RC model is used to model battery in this paper. As shown in Fig. 1 (b), the first-order RC model consists of three parts: (i) The voltage source, which is parameterized as a function of battery SOC; (ii) The equivalent ohmic resistance R_0; (iii) The parallel connected RC network, including R_1 and C_1, present the mass transport effect and dynamic voltage performance of the battery. U_1 is the voltage over the RC network. V_p is the voltage over the equivalent ohmic resistance and RC network. V_t is the battery voltage. I_L is the battery current.

The discrete state space function of first-order RC model can be expressed as

$$\begin{cases} x_k = A_{k-1}x_{k-1} + B_{k-1}I_{L,k-1} \\ V_t = \mathrm{F}(x_k, I_{L,k}) \end{cases}, \tag{1}$$

where

$$\begin{cases} x_k = [U_{1,k}\ SOC_k]^T \\ A_{k-1} = \begin{bmatrix} \varphi_{1,k-1} & 0 \\ 0 & 1 \end{bmatrix} \\ B_{k-1} = \left[R_{1,k-1}(1-\varphi_{1,k-1})\dfrac{T_s}{3600Q_c}\right]^T \\ \mathrm{F}(x_k, I_{L,k}) = \mathrm{U_{ocv}}(SOC_k) + R_{0,k}I_{L,k} + U_{1,k} \\ \varphi_{1,k-1} = \exp\left(-\dfrac{T_s}{R_{1,k-1}C_{1,k-1}}\right) \end{cases}, \tag{2}$$

T_s is sampling time, and Q_c is battery capacity.

In order to get OCV-SOC relationship and the real capacity of the battery, the low-rate OCV test and the incremental OCV test [59] are conducted at 25 °C. In the low-rate OCV test, the battery is charged and discharged under 0.02C (0.058 A), the low-rate average OCV is calculated from the average of low-rate charge and discharge voltages. The charge capacity at 25 °C in low-rate charge is treated as real capacity of the battery. After charging to 100% SOC with low rate 0.02C and resting for 3 h, the incremental OCV test is conducted. The battery is discharged 2.5% SOC using a 0.5C pulse current with rest amount of time after discharge. Repeating this pulse current relaxation duration 40 times, the rest time duration after discharge is 2 h when SOC is greater than 10%, but 4 h when SOC is less than 10%, as the voltage drop is relatively greater in low SOC section. Then the battery is charged by the same procedure to 100% SOC with a positive pulse current. The battery voltages at the end of rest are named incremental charge OCV or incremental discharge OCV. The averages of incremental charge OCV and incremental discharge OCV are named incremental average OCV. The results of the low-rate OCV test and the incremental OCV test are shown in Fig. 1 (c). The discrepancy between low-rate average OCV and the cubic interpolation of incremental average OCV in most section is small except at the high and low SOC sections. Because the polarization voltage of battery at beginning of low-rate charge or discharge is smaller than the ending of low-rate charge or discharge, and cannot mutually offset in calculation of the average OCV at the high or low SOC sections, the cubic interpolation of incremental average OCV is used in this research to fit OCV-SOC curve of the battery.

2.3. Offline model identification by genetic algorithm

In the experiments, the dynamic stress test (DST) current profile is employed to investigate the dynamic electric behavior of the battery. At the first 10 min in the current profiles, the current is kept at 0 A, then repeats DST cycles 30 times. The whole current profile is shown in Fig. 2 (a), one completed DST cycle is shown in Fig. 2 (b), the maximum discharge current is scaled to 5.8 A (2C), and the corresponding measured battery voltage is shown Fig. 2 (c). The temperature of the temperature chamber is set to 25 °C in testing. Before the DST, the battery is fully charged by CCCV method (the cutoff current is 0.02 C) and rests for 3 h before loading current profiles. The current and voltage profiles, in Fig. 2(a)–(c), are used as the data set for offline model identification in this section.

Both time-invariant and time-varying models are used to model the battery. The parameters of battery model are constant in time-invariant model, and are time-varying in time-varying model. The time-varying parameters are set to the cubic interpolation of 21 sample points evenly distributed within the DST cycles. The offline model identification is done by two steps for each models as follow, the ohmic resistance is identified in the first step, and the parameters in the parallel connected RC network are identified in the second step.

Step 1, for the time-invariant model, one ohmic resistance, $R_{0,c}$, and for time-varying model, 21 sample points, $R_{0,s} = [R_{0,s_1}, R_{0,s_2}, \cdots, R_{0,s_{21}}]$, are chosen as the variables to be identified by GA method. The ohmic resistance at every current change edge in the DST current profile are calculated by $R_0 = \Delta V_t/\Delta I_L$. For time-invariant model, the objective function of GA is the root mean square error (RMSE) between the calculated R_0 and $R_{0,c}$ at every current change edge. For time-varying model, the objective function of GA is the RMSE between the calculated R_0 and the cubic-interpolated R_0 by sample points $R_{0,s}$ at every current change edge. GA is used to find the $R_{0,c}$ and $R_{0,s}$ to minimize the corresponding objective function.

Step 2, the parameters in parallel connected RC network are identified. For time-invariant model, $[R_{1,c}, \varphi_{1,c}]$, and for time-varying model, $R_{1,s} = [R_{1,s_1}, \cdots, R_{1,s_{21}}]$ and $\varphi_{1,s} = [\varphi_{1,s_1}, \cdots, \varphi_{1,s_{21}}]$, are chosen as the variables to be identified by GA method. The objective function is the RMSE between battery measured voltage, V_t, and simulative voltage, V_s, calculated by the time-invariant model or the time-varying model. In calculating the simulative voltage, R_0 at query time is $R_{0,c}$ for the time-invariant model, and is the cubic interpolation of $R_{0,s}$ for the time-varying model. Both $R_{0,c}$ and $R_{0,s}$ have been identified in Step 1. In the time-varying model, R_1 and φ_1 at query time are the cubic-interpolation of $R_{1,s}$ and $\varphi_{1,s}$, respectively. If the query time is beyond the time range of the sample points, the constant extrapolation method is adopted. GA is used to find the $[R_{1,c}, \varphi_{1,c}]$ and $[R_{1,s}, \varphi_{1,s}]$ to minimize the corresponding objective function.

The identified parameters, $R_{0,c}$, $R_{1,c}$ and $\varphi_{1,c}$, of time-invariant model and the lower and upper bounds of these parameters in GA setting are shown in Table 1. The identified results, $R_{0,s}$, $R_{1,s}$ and $\varphi_{1,s}$, of time-varying model are shown in Fig. 2 (d)–(f). The markers on the curves are the sample points of the cubic-interpolation. The lower and upper bounds of these parameters in GA are also shown there. The root mean squares errors (RMSE) of modeling battery voltage with time-invariant model and time-varying model are 15.6 mV and 12.0 mV, respectively. The modeling errors are rather small relative to the range of battery voltage. The modeling errors of the time-varying model are less than that of time-invariant model, indicating that the modeling accuracy of time-varying model is higher than that of time-invariant model. Matlab® GA toolbox is employed to run the GA in this research. The settings in Matlab® GA toolbox are listed in Table 2, the rest settings of GA are default settings of the toolbox.

3. Battery model identification biases under noise corruptions

3.1. Description of the noise corruption problems

(a) Errors in variables (EIV) problem.

In parameter identification of a dynamic system, it is common that the measurements of both output and input are contaminated by the noise errors. This problem is usually called the errors in variables (EIV) problem [46–48]. A discrete-time single-input single-output (SISO) EIV system is shown in Fig. 3 (a), and described as

$$V_{p0,k} = G(q^{-1}) I_{L0,k}, \tag{3}$$

where $I_{L0,k}$ and $V_{p0,k}$ denote the system input and output, respectively, q^{-1} denotes the unit-delay operator. The transfer function $G(q^{-1})$ is described as

Table 1
Offline identification results of time-invariant model.

	$R_{0,c}$(mΩ)	$R_{1,c}$(mΩ)	$\varphi_{1,c}$
Identification result	34.1	74.1	0.9925
Upper bounds	75	250	1
Lower bounds	20	20	0.8

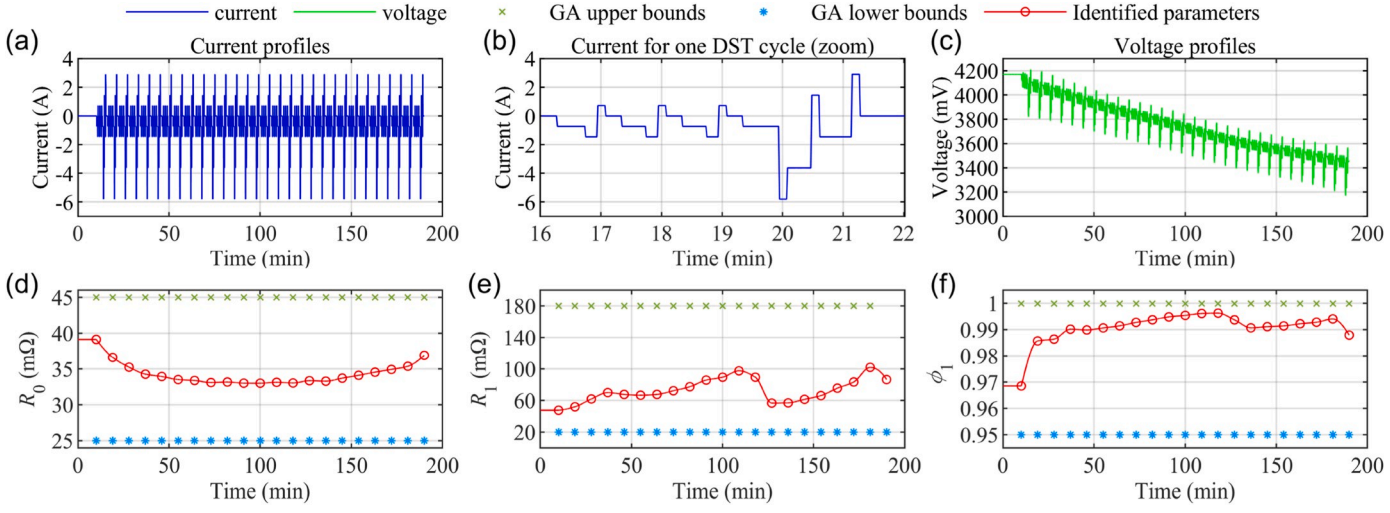

Fig. 2. (a)–(c) Measured current and voltage profiles of DST cycles; (d)–(f) offline model identification results of time-varying model.

Table 2
Settings in Matlab® GA toolbox in offline parameter identification.

Settings	Time-invariant model		Time-varying model	
	$R_{0,c}$	$[R_{1,c}, \varphi_{1,c}]$	$R_{0,s}$	$[R_{1,s}, \varphi_{1,s}]$
Variables number	1	2	21	42
Population size	2000	2000	16000	16000
Generation number	2000	2000	2000	2000
Selection function	uniform	uniform	uniform	uniform

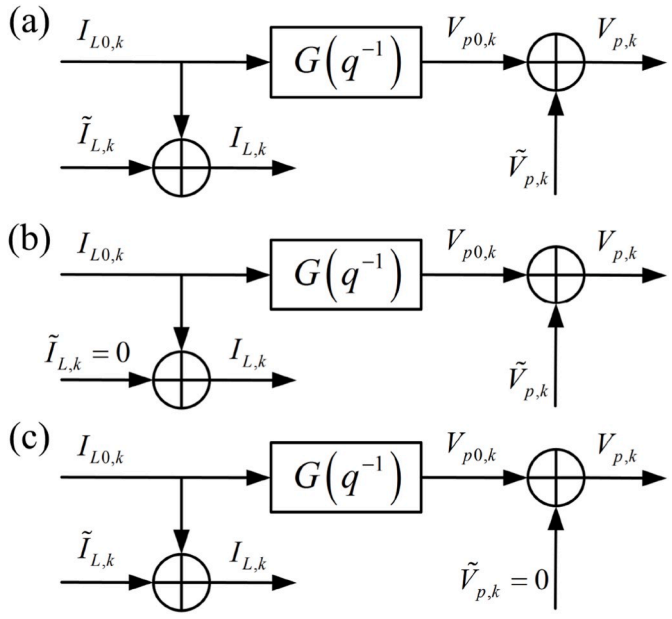

Fig. 3. A system described by (a) errors in variables (EIV) model; (b) output error (OE) model; (c) input error (IE) model.

$$G(q^{-1}) = \frac{B(q^{-1})}{A(q^{-1})} = \frac{b_1 q^{-1} + \cdots + b_m q^{-m}}{1 + a_1 q^{-1} + \cdots + a_n q^{-n}}. \tag{4}$$

The measurements of $I_{L0,k}$ and $V_{p0,k}$ are contaminated by the input and output noise $\tilde{I}_{L,k}$ and $\tilde{V}_{p,k}$, and are given by

$$I_{L,k} = I_{L0,k} + \tilde{I}_{L,k}, \tag{5}$$

$$V_{p,k} = V_{p0,k} + \tilde{V}_{p,k}, \tag{6}$$

where $\tilde{I}_{L,k}$ and $\tilde{V}_{p,k}$ are assumed to be zero-mean white noise with variances σ_I^2 and σ_V^2, respectively, independent with each other, V_{p0} and I_{L0}, as well.

The estimated parameter vector is

$$\theta^T = [a^T, b^T] = [a_1 \cdots a_n, b_1 \cdots b_m]. \tag{7}$$

The EIV system described by Eqs. (3)–(7) can be expressed in regression form,

$$V_{p,k} = \psi_k^T \theta + \tilde{V}_{L,k} - \tilde{\psi}_k^T \theta, \tag{8}$$

where

$$\psi_k^T = [-V_{p,k-1} \cdots -V_{p,k-n}, I_{L,k-1} \cdots I_{L,k-m}],$$
$$\text{and } \tilde{\psi}_k^T = [-\tilde{V}_{p,k-1} \cdots -\tilde{V}_{p,k-n}, \tilde{I}_{L,k-1} \cdots \tilde{I}_{L,k-m}];$$
$$\text{and } \psi_k = \psi_{0,k} + \tilde{\psi}_k, \tag{9}$$

where

$$\psi_{0,k}^T = [-V_{p0,k-1} \cdots -V_{p0,k-n}, I_{L0,k-1} \cdots I_{L0,k-m}].$$

(b) Output error (OE) problem

When assuming the input measurement is not contaminated by noise, or the noise imposed on input measurement is supposed to be negligible, which means $\sigma_I^2 = 0$, the EIV problem becomes output error (OE) problem, as shown in Fig. 3 (b).

(c) Input error (IE) problem

Similarly, when assuming the output measurement is not contaminated by noise, or the noise imposed on output measurement is supposed to be negligible, which means $\sigma_V^2 = 0$, the EIV problem becomes input error (IE) problem, as shown in Fig. 3 (c).

3.2. Derivation of identification biases under noise corruptions

(a) Bias formula for EIV problem

It is known that the conventional Least Squares (LS) method yields biased estimates when it is applied to identify EIV system [46–48]. The reason and the magnitude of bias caused by noise are derived as following. (cf. Ref. [48] for a detailed derivation.)

Generally, the LS estimate of θ is given by

$$\hat{\theta}_{LS}(N) = \left(\frac{1}{N}\sum_{k=1}^{N} \psi_k \psi_k^T\right)^{-1} \left(\frac{1}{N}\sum_{k=1}^{N} \psi_k V_{p,k}\right). \tag{10}$$

Substituting (8) into (10) yields

$$\hat{\theta}_{LS}(N) = \left(\frac{1}{N}\sum_{k=1}^{N} \psi_k \psi_k^T\right)^{-1} \left(\frac{1}{N}\sum_{k=1}^{N} \psi_k (\psi_k^T \theta + \tilde{V}_{p,k} - \tilde{\psi}_k^T \theta)\right)$$
$$= \theta + \left(\frac{1}{N}\sum_{k=1}^{N} \psi_k \psi_k^T\right)^{-1} \left(\frac{1}{N}\sum_{k=1}^{N} \psi_k (\tilde{V}_{p,k} - \tilde{\psi}_k^T \theta)\right). \tag{11}$$

$$\text{Defining } R = E[\psi_k \psi_k^T] = \lim_{N\to\infty} \hat{R}_N = \lim_{N\to\infty} \frac{1}{N}\sum_{k=1}^{N} \psi_k \psi_k^T, \tag{12}$$

and letting $N \to \infty$ in (11),

$$\hat{\theta}_{LS}(N) = \theta + R^{-1} E[\psi_k (\tilde{V}_{p,k} - \tilde{\psi}_k^T \theta)]. \tag{13}$$

Since $\tilde{I}_{L,k}$ and $\tilde{V}_{p,k}$ are white noises, and $\tilde{I}_{L,k}$, $\tilde{V}_{p,k}$, $V_{p0,k}$ and $I_{L0,k}$ are mutually independent,

$$\begin{aligned} &E[\psi_k (\tilde{V}_{p,k} - \tilde{\psi}_k^T \theta)] \\ &= E[(\psi_{0,k} + \tilde{\psi}_k)(\tilde{V}_{p,k} - \tilde{\psi}_k^T \theta)] \\ &= E[\psi_{0,k} \tilde{V}_{p,k}] + E[\tilde{\psi}_k \tilde{V}_{p,k}] - E[\psi_{0,k} \tilde{\psi}_k^T]\theta - E[\tilde{\psi}_k \tilde{\psi}_k^T]\theta, \\ &= 0 + 0 - 0 - D_{EIV}\theta \\ &= -D_{EIV}\theta \end{aligned} \tag{14}$$

$$\text{where } D_{EIV} = \text{diag}\{\sigma_V^2 I_{n\times n}; \sigma_I^2 I_{m\times m}\}. \tag{15}$$

From Eq. (13), it is known that the estimation is given by

$$\hat{\theta}_{LS,EIV}(N) = \theta - R^{-1} D_{EIV} \theta. \tag{16}$$

$$\text{Defining } P = \lim_{N\to\infty} \hat{P}_N = \lim_{N\to\infty} \left(\sum_{k=1}^{N} \psi_k \psi_k^T\right)^{-1}, \tag{17}$$

according to Eq. (12), we can get

$$R^{-1} = NP. \tag{18}$$

Eq. (16) can be written as

$$\widehat{\theta}_{LS,EIV}(N) = \theta - NPD_{EIV}\theta, \tag{19}$$

where $D_{EIV} = \mathrm{diag}\{\sigma_V^2 I_{n\times n}; \sigma_I^2 I_{m\times m}\}$. (20)

Let the matrix P be partitioned as

$$P = \begin{bmatrix} P^{11} & P^{12} \\ P^{21} & P^{22} \end{bmatrix}, \tag{21}$$

where $P^{11} \in \mathbb{R}^{n\times n}$ and $P^{22} \in \mathbb{R}^{m\times m}$.

Eq. (19) can be written as

$$\widehat{\theta}_{LS,EIV}(N) = \theta - \begin{bmatrix} NP^{11}\sigma_V & NP^{12}\sigma_I \\ NP^{21}\sigma_V & NP^{22}\sigma_I \end{bmatrix}\theta. \tag{22}$$

(b) Bias formula for OE problem

For OE problem, by setting $\sigma_I^2 = 0$, as assumed the input measurement is not contaminated by noise, according to Eq. (19), the bias formula is

$$\widehat{\theta}_{LS,OE}(N) = \theta - NPD_{OE}\theta, \tag{23}$$

where $D_{OE} = \mathrm{diag}\{\sigma_V^2 I_{n\times n}; 0_{m\times m}\}$. (24)

Substituting Eq. (21) and Eq. (24) into Eq. (23) leads to

$$\widehat{\theta}_{LS,OE}(N) = \theta - \begin{bmatrix} NP^{11}\sigma_V & 0_{n\times m} \\ NP^{21}\sigma_V & 0_{m\times m} \end{bmatrix}\theta. \tag{25}$$

(c) Bias formula for IE problem

For IE problem, by setting $\sigma_V^2 = 0$, as assumed the output measurement is not contaminated by noise, according to Eq. (19), the bias formula is

$$\widehat{\theta}_{LS,IE}(N) = \theta - NPD_{IE}\theta, \tag{26}$$

where $D_{IE} = \mathrm{diag}\{0_{n\times n}; \sigma_I^2 I_{m\times m}\}$. (27)

Substituting Eq. (21) and Eq. (27) into Eq. (26) leads to

$$\widehat{\theta}_{LS,IE}(N) = \theta - \begin{bmatrix} 0_{n\times n} & NP^{12}\sigma_I \\ 0_{m\times n} & NP^{22}\sigma_I \end{bmatrix}\theta. \tag{28}$$

In summary, according to the bias formula for EIV, OE, and IE problems, as shown in Eq. (19), Eq. (23), and Eq. (26), the presence of measurement noises in either only one of input and output measurements or both of them will result in the biases in model identification by LS.

3.3. Regression structure for system identification

For the online identification, the least squares (LS) algorithm can be transform to recursive least squares (RLS). In order to avoid data saturation phenomenon and track the time-varying parameters, the forgetting factor λ is employed in RLS to reduce the influence of the old data. This is the well-known forgetting factor recursive least squares (FRLS) [60] as shown in Table 3, where $0 < \lambda \leq 1$. When $\lambda = 1$, FRLS is equal to RLS, which gives the same weights to old and new data. When $\lambda < 1$, FRLS gives less weight to old data and more weights to new data.

Table 3
Forgetting factor recursive least squares algorithm (FRLS) [60].

$$\widehat{\theta}_k = \widehat{\theta}_{k-1} + L_{\lambda,k}\left[V_{p,k} - \psi_k^{\mathrm{T}}\widehat{\theta}_{k-1}\right] \tag{29}$$

$$L_{\lambda,k} = \frac{P_{\lambda,k-1}\psi_k}{\lambda_k + \psi_k^{\mathrm{T}}P_{\lambda,k-1}\psi_k} \tag{30}$$

$$P_{\lambda,k} = \frac{1}{\lambda_k}\left[I - L_{\lambda,k}\psi_k^{\mathrm{T}}\right]P_{\lambda,k-1} \tag{31}$$

For the system identification, defining $V_{p,k} = V_{t,k} - U_{ocv}(SOC_k)$, the discrete-time state space system of first-order RC model, as shown in Eq. (1), turns into the regression expression, which is given by

$$V_{p,k} = \theta_k^{\mathrm{T}}\psi_k = -a_{1,k}V_{p,k-1} + b_{0,k}I_{L,k} + b_{1,k}I_{L,k-1}, \tag{32}$$

where

$$\psi_k = \begin{bmatrix} \\ -V_{p,k-1} I_{L,k} I_{L,k-1} \end{bmatrix}^{\mathrm{T}}, \tag{33}$$

$$\begin{cases} \theta_k^{\mathrm{T}} = \left[a^{\mathrm{T}} b^{\mathrm{T}}\right]^{\mathrm{T}} \\ a_k^{\mathrm{T}} = [a_{1,k}] \\ b_k^{\mathrm{T}} = [b_{0,k} b_{1,k}] \end{cases}, \tag{34}$$

and

$$\begin{cases} a_{1,k} = -\varphi_{1,k} \\ b_{0,k} = R_{0,k} \\ b_{1,k} = R_{1,k} - \varphi_{1,k}R_{0,k} - \varphi_{1,k}R_{1,k} \end{cases}. \tag{35}$$

Once θ_k, in the regression model, is solved, the model parameters of the battery model are reversely deduced as

$$\begin{cases} \varphi_{1,k} = -a_{1,k} \\ R_{0,k} = b_{0,k} \\ R_{1,k} = (b_{1,k} - a_{1,k}b_{0,k})/(1 + a_{1,k}) \end{cases}. \tag{36}$$

3.4. Simulation verification for identification biases under noise corruptions

In this section, simulation studies are conducted to verify that the conventional RLS is asymptotically biased in battery model identifications for the three noise corruption problems, including OE, IE and EIV problems.

The voltage, V_p, in the simulation are created according to the discrete state space function in Eq. (1) with 1 Hz sample rate. The current profile used as input excitation to create V_p is the DST cycles profile as shown in Fig. 2 (a). The parameters of the model are the same as the identified time-invariant model in Section 2.3.

In order to evaluate the effect of noise on identification biases in different noise corruption problems, seven combinations of the white noises are imposed on the measurements of noise free battery voltage and current profiles as shown in Table 4, including the noise free case (Case 1), the only voltage measurement corrupted cases (Case 2 and Case 3), the only current measurement corrupted cases (Case 4 and Case 5), and the both voltage and current measurements corrupted cases (Case 6 and Case 7). The noises in these cases are white noise. The

Table 4
Variances of noises imposed on simulative voltage and current measurements for RLS identification.

Problem type	Case No.	Variance of noises
noise free	Case 1	$\sigma_V^2 = 0\mathrm{mV}^2, \sigma_I^2 = 0\mathrm{A}^2$
OE	Case 2	$\sigma_V^2 = 5\mathrm{mV}^2, \sigma_I^2 = 0\mathrm{A}^2$
	Case 3	$\sigma_V^2 = 10\mathrm{mV}^2, \sigma_I^2 = 0\mathrm{A}^2$
IE	Case 4	$\sigma_V^2 = 0\mathrm{mV}^2, \sigma_I^2 = 0.005\mathrm{A}^2$
	Case 5	$\sigma_V^2 = 0\mathrm{mV}^2, \sigma_I^2 = 0.01\mathrm{A}^2$
EIV	Case 6	$\sigma_V^2 = 5\mathrm{mV}^2, \sigma_I^2 = 0.005\mathrm{A}^2$
	Case 7	$\sigma_V^2 = 10\mathrm{mV}^2, \sigma_I^2 = 0.01\mathrm{A}^2$

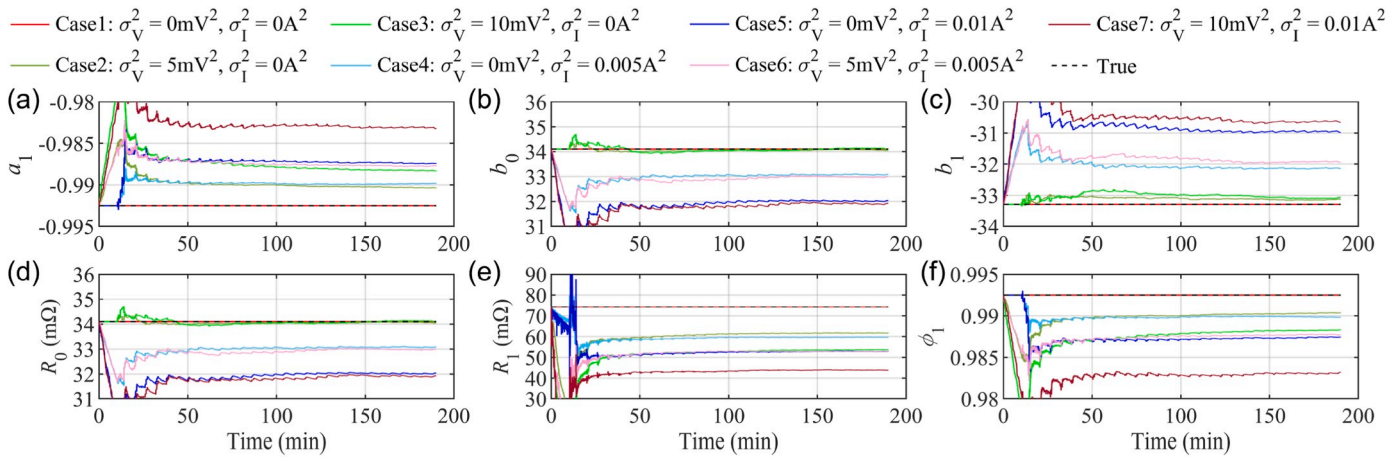

Fig. 4. Identification results of first-order RC model by conventional RLS under noise corruptions.

identification results by conventional RLS are shown in Fig. 4. As seen, in noise free case (Case 1), the identification results coincide well with the true model parameters, but identification results deviate from the true values in the cases with noise corrupted measurements. In the only voltage measurement corrupted cases (Case 2 and Case 3), even though only voltage measurements are corrupted by noises, there are obvious bias in estimation of a_1 and slight bias in estimation of b_0 and b_1. According to Eq. (36), R_1 and φ_1 are related to a_1, R_0 is related to b_0, so there are obvious biases of R_1 and φ_1, and slight bias of R_0. In the only current measurement corrupted cases (Case 4 and Case 5), there are obvious biases in estimation of all parameters. In both voltage and current measurements corrupted cases (Case 6 and Case 7), the identification of all parameters are also biased. The biases of θ (including a_1, b_0 and b_1) in Case 6 are approximately equal to the addition of the biases in Case 2 and Case 4, in which only one of voltage and current measurements is corrupted by noise with the same variance in Case 6. Similarly, the biases of θ in Case 7 are approximately equal to the addition of the biases in Case 3 and Case 5. These simulation results are consistent with the bias formulas for EIV, OE and IE problems as shown in Eq. (22), Eq. (25) and Eq. (28). It is also noticed that the biases are positive correlative with the variance of noises in these simulations.

In summary, the simulations in this section verify that the identification by RLS is biased not only when both voltage and current measurements are corrupted by noises, but also when only one of them is corrupted by noise. The biases increase with the increased noise variance. The results of simulations are consistent with the derivation of relations between the noise variances and the identification biases in the least squares as shown in Section 3.2.

4. Joint algorithm of bias compensation RLS and EKF

4.1. Bias compensation RLS for noise corrupted measurements

As shown in Eq. (19), Eq. (23) and Eq. (26), if the variances of noises imposed on voltage and current measurements can be estimated, the identification biases by RLS can be compensated. In order to estimate the variances of noises, σ_V^2 and σ_I^2, in voltage and current measurements, the first equation is derived from the minimal value of the LS cost function, and is given by (cf. Ref. [47,48] for a detailed derivation.)

$$\lim_{k\to\infty}\frac{1}{k}J_k = \lim_{k\to\infty}\frac{1}{k}\sum_{i=1}^{k}\left(V_{p,i} - \psi_i^{\mathrm{T}}\widehat{\theta}_{LS,k}\right)^2 = \sigma_V^2\left(1 + (\lim_{k\to\infty}\widehat{a}_{LS,k})^{\mathrm{T}}\widehat{a}\right) + \sigma_I^2(\lim_{k\to\infty}\widehat{b}_{LS,k})^{\mathrm{T}}\widehat{b}, \quad (37)$$

where J_k is the LS cost function, and can be recursively estimated by

$$J_k = \lambda J_{k-1} + \frac{\lambda\left(V_{p,k} - \psi_k^T\widehat{\theta}_{LS,k-1}\right)^2}{\lambda + \psi_k^T P_{\lambda,k-1}\psi_k}. \quad (38)$$

For the OE problem, as assuming the noise of current measurements is negligible, only the variance of noise in the voltage measurement, σ_V^2, is needed to be estimated. As assumed, $\sigma_I^2 = 0$, according to Eq. (37), σ_V^2 is

$$\sigma_{V,k}^2 = \frac{J_k}{k\left(1 + \widehat{a}_{LS,k}^T\widehat{a}_{k-1}\right)}. \quad (39)$$

The algorithm of forgetting factor bias compensation recursive least square for the OE problem (FBCRLSOE) can be established as summarized in Table 5.

Similarly, for the IE problem, as assuming the noise of voltage measurements is negligible, only the variance of noise in current measurement, σ_I^2, is needed to be estimated. As assumed, $\sigma_V^2 = 0$, according

Table 5
Algorithm of forgetting factor bias compensation recursive least square for OE problem (FBCRLSOE) [54].

$$\widehat{\theta}_{LS,k} = \widehat{\theta}_{LS,k-1} + L_{\lambda,k}\left[V_{p,k} - \psi_k^T\widehat{\theta}_{LS,k-1}\right] \quad (40)$$

$$L_{\lambda,k} = \frac{P_{\lambda,k-1}\psi_k}{\lambda + \psi_k^T P_{\lambda,k-1}\psi_k} \quad (41)$$

$$P_{\lambda,k} = \frac{1}{\lambda}\left[\mathrm{I} - L_{\lambda,k}\psi_k^T\right]P_{\lambda,k-1} \quad (42)$$

$$J_k = \lambda J_{k-1} + \frac{\lambda\left(V_{p,k} - \psi_k^T\widehat{\theta}_{LS,k-1}\right)^2}{\lambda + \psi_k^T P_{\lambda,k-1}\psi_k} \quad (43)$$

$$\sigma_{V,k}^2 = \frac{J_k}{k(1 + \widehat{a}_{LS,k}^T\widehat{a}_{k-1})} \quad (44)$$

$$D_{OE} = \mathrm{diag}\{\sigma_V^2 I_{n\times n}; 0_{m\times m}\} \quad (45)$$

$$\widehat{\theta}_k = \widehat{\theta}_{LS,k} + kP_{\lambda,k}D_{OE}\widehat{\theta}_{k-1} \quad (46)$$

to Eq. (37), σ_I^2 is

$$\sigma_{I,k}^2 = \frac{J_k}{k\widehat{b}_{LS,k}^T \widehat{b}_{k-1}}. \tag{47}$$

Table 6
Algorithm of forgetting factor bias compensation recursive least square for IE problem (FBCRLSIE).

$$\widehat{\theta}_{LS,k} = \widehat{\theta}_{LS,k-1} + L_{\lambda,k}\left[V_{p,k} - \psi_k^T \widehat{\theta}_{LS,k-1}\right] \tag{48}$$

$$L_{\lambda,k} = \frac{P_{\lambda,k-1}\psi_k}{\lambda + \psi_k^T P_{\lambda,k-1}\psi_k} \tag{49}$$

$$P_{\lambda,k} = \frac{1}{\lambda}\left[I - L_{\lambda,k}\psi_k^T\right]P_{\lambda,k-1} \tag{50}$$

$$J_k = \lambda J_{k-1} + \frac{\lambda\left(V_{p,k} - \psi_k^T \widehat{\theta}_{LS,k-1}\right)^2}{\lambda + \psi_k^T P_{\lambda,k-1}\psi_k} \tag{51}$$

$$\sigma_{I,k}^2 = \frac{J_k}{k\widehat{b}_{LS,k}^T \widehat{b}_{k-1}} \tag{52}$$

$$D_{IE} = \mathrm{diag}\left\{0_{n\times n}; \sigma_I^2 I_{m\times m}\right\} \tag{53}$$

$$\widehat{\theta}_k = \widehat{\theta}_{LS,k} + kP_{\lambda,k}D_{IE}\widehat{\theta}_{k-1} \tag{54}$$

The algorithm of forgetting factor bias compensation recursive least square for the IE problem (FBCRLSIE) can be established as summarized in Table 6.

For the EIV problem, both the variances of noises in output and input are needed to be estimated, so at least two equations are needed. A method to estimate σ_V^2 and σ_I^2 is proposed in Ref. [48], by augmenting a zero parameter in the numerator of the system transfer function, which gives the following augmented transfer function,

$$\overline{G}\left(q^{-1}\right) = \frac{\overline{B}(q^{-1})}{A(q^{-1})} = \frac{b_1 q^{-1} + \cdots + b_m q^{-m} + b_{m+1} q^{-(m+1)}}{1 + a_1 q^{-1} + \cdots + a_n q^{-n}}, \tag{55}$$

with

$$\overline{\theta}^T = \left[a^T, \overline{b}^T\right], \tag{56}$$

$$\overline{b}^T = [b_1 \cdots b_m b_{m+1}] = \left[b^T 0\right]. \tag{57}$$

It is notable that the augmented transfer function is equivalent to the original transfer function, as $b_{m+1} = 0$. This constrain can be expressed as

$$\overline{H}^{\mathrm{T}}\overline{\theta} = 0, \tag{58}$$

where

$$\overline{H}^{\mathrm{T}} = \left[0^{\mathrm{T}}, \overline{h}^{\mathrm{T}}\right] \in \mathbb{R}^{n+m+1}, \tag{59}$$

$$h^T = [0 \cdots 01] \in \mathbb{R}^{m+1}. \tag{60}$$

Premultiplying $\widehat{\theta}_{LS}(k) = \overline{\theta} - k\overline{PD}_{EIV}\overline{\theta}$ with $\overline{H}^{\mathrm{T}}$ yields

$$\overline{H}^{\mathrm{T}} k\overline{PD}_{EIV}\overline{\theta} = -\overline{H}^{\mathrm{T}}\overline{\theta}_{LS}(k). \tag{61}$$

Let the matrix $\overline{P}$ be partitioned as

$$\overline{P} = \begin{bmatrix} \overline{P}^{11} & \overline{P}^{12} \\ \overline{P}^{21} & \overline{P}^{22} \end{bmatrix}, \tag{62}$$

where $\overline{P}^{11} \in \mathbb{R}^{n\times n}$ and $\overline{P}^{22} \in \mathbb{R}^{(m+1)\times(m+1)}$.

Substituting (20), (59), (60) and (62) into (61) leads to the second equation to solve σ_V^2 and σ_I^2,

$$k\sigma_V^2 \overline{h}^{\mathrm{T}}\overline{P}^{21}\widehat{a} + k\sigma_I^2 \overline{h}^{\mathrm{T}}\overline{P}^{22}\overline{b} = -\overline{h}^{\mathrm{T}}\overline{b}_{LS}. \tag{63}$$

Defining

$$\begin{aligned} \overline{\psi}_k^T &= \left[\psi_k^T I_{L,k-m-1}\right] \\ &= [\\ &\quad -V_{p,k-1} \cdots \\ &\quad -V_{p,k-n} I_{L,k-1} \cdots I_{L,k-m-1}]. \end{aligned} \tag{64}$$

The algorithm of forgetting factor bias compensation recursive least square for EIV problem (FBCRLSEIV) is summarized in Table 7.

4.2. Joint algorithms of RLS-based method and extended Kalman filter

The joint RLS-based method and extended Kalman filter (EKF) is widely used in parameter and state co-estimation [40,44,61,62], referred as RLS-based-EKF hereafter. The framework of RLS-based-EKF is shown in Fig. 5. In RLS-based-EKF method, the battery model is on-line identified by RLS-based method and the SOC is observed by EKF in a dual sequential framework. The EKF algorithm is shown in Table 8. To

Table 7
Algorithm of forgetting factor bias compensation recursive least square for EIV problem (FBCRLSEIV) [47,48].

$$\overline{\theta}_{LS,k} = \overline{\theta}_{LS,k-1} + \overline{L}_{\lambda,k}\left[V_{p,k} - \overline{\psi}_k^T \overline{\theta}_{LS,k-1}\right] \tag{65}$$

$$\overline{L}_{\lambda,k} = \frac{\overline{P}_{\lambda,k-1}\overline{\psi}_k}{\lambda + \overline{\psi}_k^T \overline{P}_{\lambda,k-1}\overline{\psi}_k} \tag{66}$$

$$\overline{P}_{\lambda,k} = \frac{1}{\lambda}\left[I - \overline{L}_{\lambda,k}\overline{\psi}_k^T\right]\overline{P}_{\lambda,k-1} \tag{67}$$

$$\overline{J}_k = \lambda\overline{J}_{k-1} + \frac{\lambda\left(V_{p,k} - \overline{\psi}_k^T \overline{\theta}_{LS,k-1}\right)^2}{\lambda + \overline{\psi}_k^T \overline{P}_{\lambda,k-1}\overline{\psi}_k} \tag{68}$$

$$\overline{P}_{\lambda,k} = \begin{bmatrix} \overline{P}_{\lambda,k}^{11} & \overline{P}_{\lambda,k}^{12} \\ \overline{P}_{\lambda,k}^{21} & \overline{P}_{\lambda,k}^{22} \end{bmatrix}, \overline{P}_{\lambda,k}^{11} \in \mathbb{R}^{n\times n}, \overline{P}_{\lambda,k}^{22} \in \mathbb{R}^{(m+1)\times(m+1)} \tag{69}$$

$$\begin{bmatrix} 1 + \widehat{a}_{LS,k}^{\mathrm{T}}\widehat{a}_{k-1} & \overline{b}_{LS,k}^{\mathrm{T}}\overline{b}_{k-1} \\ k\overline{h}^{\mathrm{T}}\overline{P}_{\lambda,k}^{21}\widehat{a}_{k-1} & k\overline{h}^{\mathrm{T}}\overline{P}_{\lambda,k}^{22}\overline{b}_{k-1} \\ -\overline{h}^{\mathrm{T}}\overline{b}_{LS,k} \end{bmatrix} \begin{bmatrix} \sigma_V^2 \\ \sigma_I^2 \end{bmatrix} = \begin{bmatrix} \frac{1}{k}\overline{J}_k \end{bmatrix} \tag{70}$$

$$\overline{D}_{EIV} = \mathrm{diag}\left\{\sigma_V^2 I_{n\times n}; \sigma_I^2 I_{(m+1)\times(m+1)}\right\} \tag{71}$$

$$\overline{\theta}_k = \overline{\theta}_{LS,k} + k\overline{P}_{\lambda,k}\overline{D}_{EIV}\overline{\theta}_{k-1} \tag{72}$$

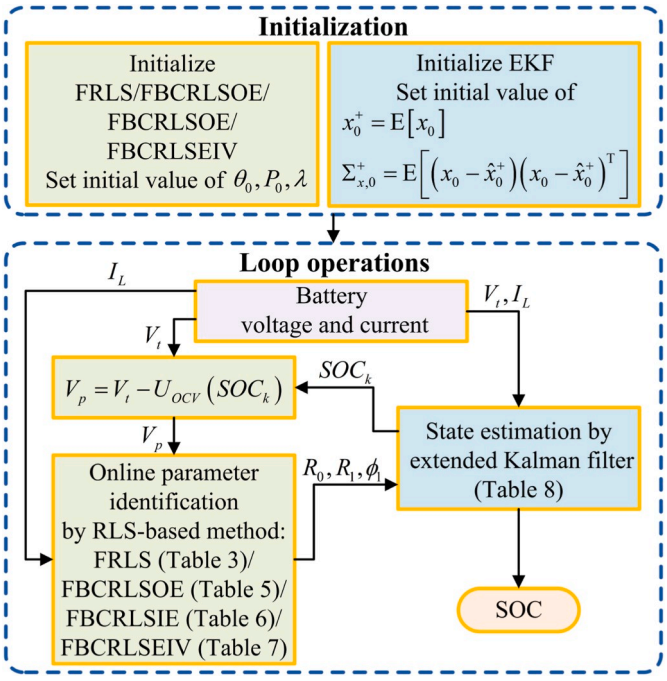

Fig. 5. The schematic of co-estimation by joint RLS-based method and extended Kalman filter (RLS-based-EKF).

identify the model by RLS-based method, the voltage over the equivalent ohmic resistance and RC network is defined as $V_p = V_t - U_{ocv}(SOC)$. V_p is calculated by the battery voltage and SOC estimated by EKF. The model used in EKF is identified by RLS-based method. Beside conventional FRLS, three bias compensation RLS methods detailed in Section 4.1 are used for online model identification. The joint FRLS and EKF co-estimation algorithm is referred as FRLS-EKF; the joint FBCRLSOE and EKF co-estimation algorithm is referred as FBCRLSOE-EKF; the joint FBCRLSIE and EKF co-estimation algorithm is referred as FBCRLSIE-EKF; the joint FBCRLSEIV and EKF co-estimation algorithm is referred as FBCRLSEIV-EKF hereafter.

As shown in Section 3, there are model identification biases in conventional RLS under noise corrupted measurements. Further, the bias estimation of model parameters will result in the deviation of SOC estimation in model-based SOC estimation methods. As the bias compensation RLS can compensate the model identification biases caused by the noise imposed on voltage or current measurements, it can be inferred that, in co-estimation, identifying model by bias compensation RLS can enhance the parameter and SOC estimation accuracy comparing to identifying model by conventional RLS under noise corrupted measurements. This inference is verified by simulation and experiment studies in the following Section 5 and Section 6.

4.3. Arithmetic operation requirements

To evaluate the computation costs of the proposed algorithms, the number of arithmetic operations required by FRLS, FBCRLSOE, FBCRLSIE, FBCRLSEIV and EKF for one iteration are listed in Tables 9–13, respectively, where rough matrix-based implementation is used. In these tables, n_θ, n_a and n_b are the dimensions of the parameter vectors θ, a and b, respectively. $n_{\overline{\theta}}$ and $n_{\overline{b}}$ are the dimensions of the augment parameter vector $\overline{\theta}$ and $n_{\overline{b}}$, in FBCRLSEIV. n_s, n_i and n_m are the dimensions of the state vectors, the input vector and the measurement vector in EKF, respectively. For first-order RC model, $n_\theta = 3$, $n_{\overline{\theta}} = 4$, $n_a = 1$, $n_b = 2$, $n_{\overline{b}} = 3$, $n_s = 2$, $n_i = 1$, $n_m = 1$. As seen in Table 14, the total number of the arithmetic operations for one iteration is 210 for FRLS-EKF, 281 for FBCRLSOE-EKF, 282 for FBCRLSIE-EKF and 505 for FBCRLSEIV-EKF, which roughly means the computation costs of FBCRLSOE-EKF, FBCRLSIE-EKF and FBCRLSEIV-EKF are 1.34, 1.34 and 2.40 times of that of FRLS-EKF. It shows that, compared with FRLS-EKF, the computation costs of FBCRLSOE-EKF and FBCRLSIE-EKF increase slightly, and that of FBCRLSEIV-EKF increases relatively more, but still not dramatically. Thus, comparing with conventional RLS, the proposed bias compensation RLS based co-estimation algorithm can also be used in online application with moderate growth in computation cost.

5. Simulation study

5.1. Simulation setting

To assess the performances of RLS-based-EKF co-estimation algorithms under noise corrupted measurements, eight simulations are conducted. The simulative battery voltages are created by the discrete state space function of the first-order RC model presented in Eq. (1), with 1 Hz sample rate. The input current profile is the same as the current profile shown in Fig. 2 (a) in Section 2.3. Both time-invariant and time-varying model, offline identified in Section 2.3, are implemented to create simulative battery voltages. Time-invariant model is implemented in Simulation 1 to Simulation 4. While, time-varying

Table 8
Algorithm of extended Kalman filter (EKF) [16].

Nonlinear state space model

$$\begin{cases} x_k = A_{k-1}x_{k-1} + B_{k-1}I_{L,k-1} + w_{k-1} \\ V_t = F(x_k, I_{L,k}) + v_k \end{cases} \quad (73)$$

Where w_k and v_k are independent, zero mean, Gaussian noise,

$$\begin{aligned} Cov(w_k, w_j) &= \Sigma_w \delta_{kj} \\ Cov(v_k, v_j) &= \Sigma_v \delta_{kj} \end{aligned} \quad (74)$$

Definitions

$$C_k = \left.\frac{\partial F(x_k, I_{L,k})}{\partial x_k}\right|_{x_k = \widehat{x_k^-}} \quad (75)$$

Initialization
For $k = 0$, set

$$\begin{aligned} x_0^+ &= E[x_0] \\ \Sigma_{x,0}^+ &= E\left[(x_0 - \widehat{x}_0^+)(x_0 - \widehat{x}_0^+)^{\mathrm{T}}\right] \end{aligned} \quad (76)$$

Computation
For $k = 1, 2, \cdots$, compute
Time update

$$\widehat{x}_k^- = A_{k-1}\widehat{x}_{k-1}^+ + B_{k-1}I_{L,k-1} \quad (77)$$

$$\Sigma_{x,k}^- = A_{k-1}\Sigma_{x,k-1}^+ A_{k-1}^{\mathrm{T}} + \Sigma_w \quad (78)$$

Measurement update

$$K_k = \Sigma_{x,k}^- C_k^{\mathrm{T}}\left[C_k \Sigma_{x,k}^- C_k^{\mathrm{T}} + \Sigma_v\right]^{-1} \quad (79)$$

$$\widehat{x}_k^+ = \widehat{x}_k^- + K_k\left[V_t - F(\widehat{x}_k^-, I_{L,k})\right] \quad (80)$$

$$\Sigma_{x,k}^+ = (I - K_k C_k)\Sigma_{x,k}^- \quad (81)$$

Table 9
FRLS arithmetic operation requirements ($n_\theta = 3$).

	Multiplication	Division	Addition
$\widehat{\theta}_k$	$2n_\theta$ (6)	0	$2n_\theta$ (6)
L_k	$2n_\theta^2 + n_\theta$ (21)	1	$2n_\theta^2 - n_\theta$ (15)
P_k	$n_\theta^3 + 2n_\theta^2$ (45)	1	$n_\theta^3 + n_\theta^2$ (36)
Total	$n_\theta^3 + 4n_\theta^2 + 3n_\theta$ (72)	2	$n_\theta^3 + 3n_\theta^2 + n_\theta$ (57)

Table 10
FBCRLSOE arithmetic operation requirements ($n_\theta = 3, n_a = 1$).

	Multiplication	Division	Addition
$\widehat{\theta}_k$	$2n_\theta$ (6)	0	$2n_\theta$ (6)
L_k	$2n_\theta^2 + n_\theta$ (21)	1	$2n_\theta^2 - n_\theta$ (15)
P_k	$n_\theta^3 + 2n_\theta^2$ (45)	1	$n_\theta^3 + n_\theta^2$ (36)
J_k	$n_\theta^2 + 2n_\theta + 3$ (18)	1	$n_\theta^2 + n_\theta$ (12)
σ_V^2	$n_a + 1$ (2)	1	n_a (1)
$\widehat{\theta}_{c,k}$	$2n_\theta^2 + n_\theta$ (21)	0	$2n_\theta^2 - n_\theta$ (15)
Total	$n_\theta^3 + 7n_\theta^2 + 6n_\theta + n_a + 4$ (113)	4	$n_\theta^3 + 6n_\theta^2 + n_\theta + n_a$ (85)

Table 11
FBCRLSIE arithmetic operation requirements ($n_\theta = 3, n_b = 2$).

	Multiplication	Division	Addition
$\widehat{\theta}_k$	$2n_\theta$ (6)	0	$2n_\theta$ (6)
L_k	$2n_\theta^2 + n_\theta$ (21)	1	$2n_\theta^2 - n_\theta$ (15)
P_k	$n_\theta^3 + 2n_\theta^2$ (45)	1	$n_\theta^3 + n_\theta^2$ (36)
J_k	$n_\theta^2 + 2n_\theta + 3$ (18)	1	$n_\theta^2 + n_\theta$ (12)
σ_I^2	$n_b + 1$ (3)	1	$n_b - 1$ (1)
$\widehat{\theta}_{c,k}$	$2n_\theta^2 + n_\theta$ (21)	0	$2n_\theta^2 - n_\theta$ (15)
Total	$n_\theta^3 + 7n_\theta^2 + 6n_\theta + n_b + 4$ (114)	4	$n_\theta^3 + 6n_\theta^2 + n_\theta + n_b - 1$ (85)

model is implemented in Simulation 5 to Simulation 8. The variances of noises and model types in simulations are listed in Table 15. As seen, four combinations of white noises are imposed on simulative battery voltages and currents, which corresponding to the noise-free, the OE, the IE and the EIV problems, respectively.

5.2. Simulation results and discussions

The conventional FRLS-EKF and the proposed bias compensation RLS based co-estimation algorithms are used to co-estimate the state and parameters in simulations with different noises and models as listed in Table 15. The forgetting factors in these algorithms are set to 0.995. In the FBCRLSEIV-EKF algorithm, in order to improve the stability, the FRLS, instead of FBCRLSEIV, is used for estimating the first 15 min data. The estimation results of the simulations with time-invariant model are shown in Fig. 6, and these with time-varying model are shown in Fig. 7.

Table 13
EKF arithmetic operation requirements ($n_s = 2, n_i = 1, n_m = 1$).

	Multiplication	Division	Addition
$\widehat{x}_k^-$	$n_s^2 + n_s n_i$ (6)	0	$n_s^2 + n_s n_i - n_s$ (4)
$\Sigma_{x,k}^-$	$2n_s^3$ (16)	0	$2n_s^3 - n_s^2$ (12)
K_k	$n_s^2 n_m + 2n_s n_m^2 + n_m^3 - n_m$(8)	$\frac{n_m(n_m+1)}{2}$ (1)	$n_s^2 n_m + 2n_s n_m^2 + n_m(n_m-1)^2 - 2n_s n_m$ (4)
$F(\widehat{x}_k^-, I_{t,k})$	1	0	2
$\widehat{x}_k^+$	$n_s n_m$ (2)	0	$n_s n_m + n_m$ (3)
$\Sigma_{x,k}^+$	$n_s^2 n_m + n_s^3$ (12)	0	$n_s^2 n_m + n_s^3 - n_s^2$ (8)
Total	45	1	33

Table 14
Total arithmetic operation requirements of RLS-based-EKF.

	Multiplication	Division	Addition	Total
FRLS-EKF	117	3	90	210
FBCRLSOE-EKF	158	5	118	281
FBCRLSIE-EKF	159	5	118	282
FBCRLSEIV-EKF	281	8	214	503

The RMSEs of the estimation results are used to evaluate the estimation accuracy as listed in Table 16.

The estimation results by FRLS-EKF are shown in Fig. 6 (a)–(d), Fig. 7 (a) – (d) and Table 16. As seen, the noises imposed on the voltage or current measurements can generate model identification biases and increase SOC estimation errors in simulations with either time-invariant or time-varying model. In the noise free simulations (Simulation 1 and Simulation 5), the estimation results are closer to the true values compared with other noise corrupted simulations. In the only voltage measurement corrupted simulations (Simulation 2 and Simulation 6), corresponding to OE problem, the RMSE of R_0 increases slightly, and the RMSEs of R_1 and φ_1 increase obviously in the both simulations; the RMSE of the SOC increases to 1.1298% in Simulation 2 and to 1.2824% in Simulation 6. In the only current measurement corrupted simulations (Simulation 3 and Simulation 7), corresponding to IE problem, the RMSEs of all parameters increase obviously in the both simulations; the RMSE of SOC increases to 1.2417% in Simulation 3 and to 1.3486% in Simulation 7. In the both voltage and current measurements corrupted simulations (Simulation 4 and Simulation 8), corresponding to EIV problem, the RMSEs of all parameters increase more greatly in all simulations; the RMSE of SOC increases to 1.6809% in Simulation 4 and to 1.8153% in Simulation 8.

The estimation results by FBCRLSOE-EKF are shown in Fig. 6 (e)–(h), Fig. 7 (e) – (h) and Table 16. As seen, in the only voltage measurement corrupted simulations (Simulation 2 and Simulation 6), even though the voltage measurements are corrupted by noises, compared with noise free simulations, the RMSEs of the SOC and the parameters increase very slightly and much less than the estimation by FRLS-EKF. It verifies that the FBCRLSOE-EKF can compensate the model identification biases and

Table 12
FBCRLSEIV arithmetic operation requirements ($n_{\bar{\theta}} = 4, n_a = 1, n_{\bar{b}} = 3$).

	Multiplication	Division	Addition
$\overline{\theta}_{ts,k}$	$2n_{\bar{\theta}}$ (8)	0	$2n_{\bar{\theta}}$ (8)
$\overline{L}_{\lambda,k}$	$2n_{\bar{\theta}}^2 + n_{\bar{\theta}}$ (36)	1	$2n_{\bar{\theta}}^2 - n_{\bar{\theta}}$ (28)
$\overline{P}_k$	$n_{\bar{\theta}}^3 + 2n_{\bar{\theta}}^2$ (96)	1	$n_{\bar{\theta}}^3 + n_{\bar{\theta}}^2$ (80)
$\overline{J}_k$	$n_{\bar{\theta}}^2 + 2n_{\bar{\theta}} + 3$ (27)	1	$n_{\bar{\theta}}^2 + n_{\bar{\theta}}$ (20)
$\begin{bmatrix}\sigma_V^2\\ \sigma_I^2\end{bmatrix}$	$n_a n_{\bar{b}} + n_{\bar{b}}^2 + n_a + 4n_{\bar{b}} + 8$ (33)	4	$n_a n_{\bar{b}} + n_{\bar{b}}^2 + n_a + 2n_{\bar{b}} - 2$ (17)
$\overline{\theta}_{c,k}$	$2n_{\bar{\theta}}^2 + n_{\bar{\theta}}$ (36)	0	$2n_{\bar{\theta}}^2 - n_{\bar{\theta}}$ (28)
Total	$n_{\bar{\theta}}^3 + 7n_{\bar{\theta}}^2 + 6n_{\bar{\theta}} + n_a n_{\bar{b}} + n_{\bar{b}}^2 + n_a + 4n_{\bar{b}} + 11$ (236)	7	$n_{\bar{\theta}}^3 + 6n_{\bar{\theta}}^2 + n_{\bar{\theta}} + n_a n_{\bar{b}} + n_{\bar{b}}^2 + n_a + 2n_{\bar{b}} - 2$ (181)

Table 15
Variances of noises imposed on battery voltage and current measurements in simulations.

Model type	Simulation No.	Problem type	Variance of noises
Time-invariant	Simulation 1	noise free	$\sigma_V^2 = 0\text{mV}^2, \sigma_I^2 = 0\text{A}^2$
	Simulation 2	OE	$\sigma_V^2 = 10\text{mV}^2, \sigma_I^2 = 0\text{A}^2$
	Simulation 3	IE	$\sigma_V^2 = 0\text{mV}^2, \sigma_I^2 = 0.01\text{A}^2$
	Simulation 4	EIV	$\sigma_V^2 = 10\text{mV}^2, \sigma_I^2 = 0.01\text{A}^2$
Time-varying	Simulation 5	noise free	$\sigma_V^2 = 0\text{mV}^2, \sigma_I^2 = 0\text{A}^2$
	Simulation 6	OE	$\sigma_V^2 = 10\text{mV}^2, \sigma_I^2 = 0\text{A}^2$
	Simulation 7	IE	$\sigma_V^2 = 0\text{mV}^2, \sigma_I^2 = 0.01\text{A}^2$
	Simulation 8	EIV	$\sigma_V^2 = 10\text{mV}^2, \sigma_I^2 = 0.01\text{A}^2$

SOC error caused by noise imposed on voltage measurement. In other noise corrupted simulations (Simulation 3, Simulation 4, Simulation 7 and Simulation 8), due to the addition of noises on the current measurements, the RMSEs of the SOC and the parameters estimated by FBCRLSOE-EKF are slightly larger than that in only voltage measurement corrupted simulations (Simulation 2 and Simulation 6).

The estimation results by FBCRLSIE-EKF are shown in Fig. 6 (i)–(l), Fig. 7 (i) – (l) and Table 16. As seen, in the only current measurement corrupted simulations (Simulation 3 and Simulation 7), even though the current measurements are corrupted by noises, the RMSEs of the SOC and the parameters increase very slightly and much less than the estimation by FRLS-EKF. It verifies that the FBCRLSIE-EKF can compensate the model identification biases and the SOC error caused by the noise imposed on the current measurement. In other noise corrupted simulations (Simulation 2, Simulation 4, Simulation 6 and Simulation 8), due to the addition of noises on the voltage measurements, the RMSEs of the SOC and the parameters estimated by FBCRLSIE-EKF are slightly larger than that in the only current measurement corrupted simulations (Simulation 3 and Simulation 7).

The estimation results by FBCRLSEIV-EKF are shown in Fig. 6 (m)–(p), Fig. 7 (m) – (p) and Table 16. As seen the RMSEs of the SOC and the parameters increase very slightly and much less than estimation by FRLS-EKF in all kinds of noise corrupted simulations. It verifies that the FBCRLSEIV-EKF can compensate the model identification biases and the SOC error caused by noises imposed on both voltage and current measurements.

In summary, these simulations verify that the noises imposed on either one of voltage and current measurements or both of them will generate biases in model identifications and increase SOC estimation errors when conventional FRLS-EKF is used. The FBCRLSOE-EKF can effectively compensate the model identification biases and SOC estimation error caused by noises, when only voltage measurement is corrupted by noise; the FBCRLSIE-EKF can effectively compensate the model identification biases and SOC estimation error caused by noises, when only current measurement is corrupted by noise; the FBCRLSEIV-EKF can effectively compensate the model identification biases and SOC estimation error caused by the noises imposed on either one of voltage and current measurements or both of them.

6. Experiment study

6.1. Experiment setting

The simulation studies assess the performances of the conventional FRLS-EKF and the proposed bias compensation RLS based co-estimation algorithms under noise corrupted measurements with an ideal battery model. In practical applications, however, there are some model errors, such as the errors in OCV-SOC function and the unmodeled battery features. So, it is necessary to implement the conventional and the proposed algorithms on the experiment data to assess their performances in practical applications.

The presentation of experiment setup has done in Section 2.1, the current and voltage profiles used in this experiment study have detailed in Section 2.3, and shown in Fig. 2 (a)–(c). Similarly to previous simulations, as listed in Table 17, four combinations of white noises are imposed on battery voltage and current measurements, corresponding to the noise free, the OE, the IE and the EIV problems, respectively.

6.2. Experiment results and discussions

In experiments, the forgetting factors are still set to 0.995. In the FBCRLSEIV-EKF method, in order to improve the stability, the FRLS, instead of FBCRLSEIV, is used for estimating the first 15 min data. The parameters of the time-varying model offline identified in Section 2.3 are set as the reference values in these experiments. The co-estimation results in experiments are shown in Fig. 8. The RMSEs of the co-estimation results are shown in Table 18.

The estimation results by FRLS-EKF are shown in Fig. 8 (a)–(d) and

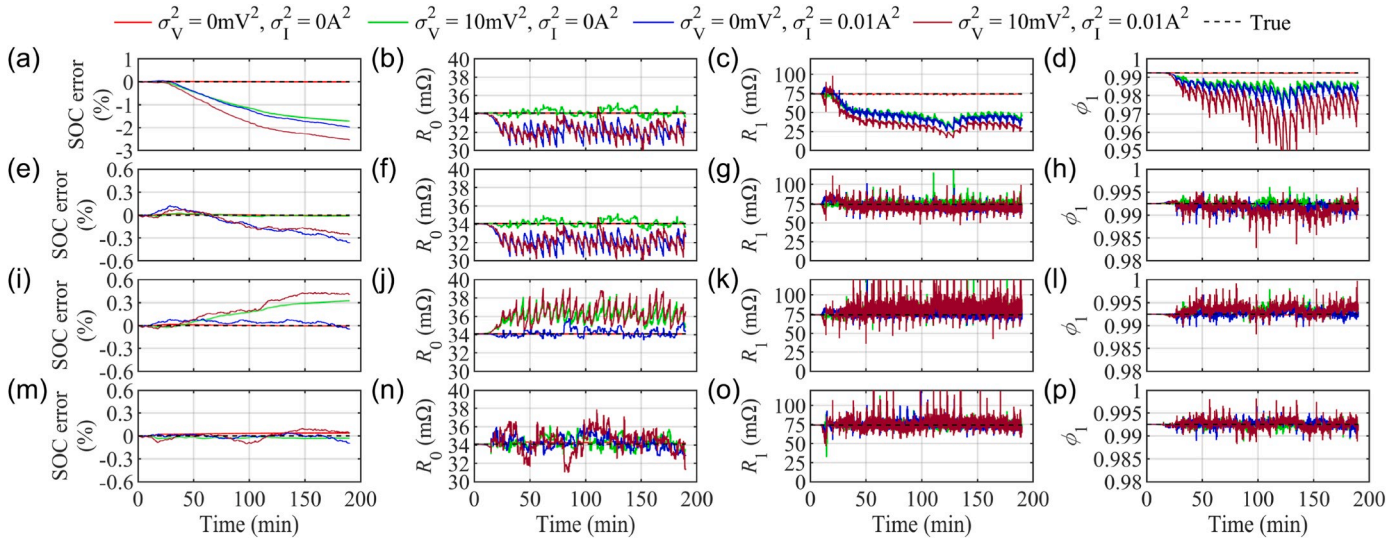

Fig. 6. Estimation results of simulations with time-invariant model under noises corrupted measurements: (a)–(d) by FRLS-EKF; (e)–(h) by FBCRLSOE-EKF; (i)–(l) by FBCRLSIE-EKF; (m)–(p) by FBCRLSEIV-EKF.

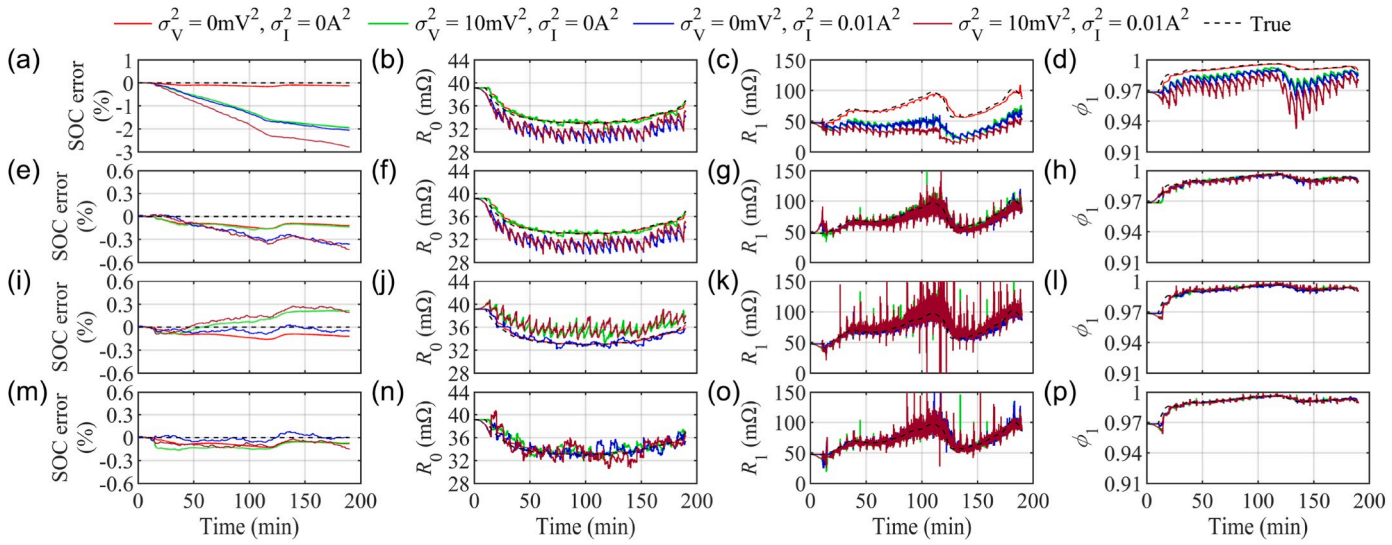

Fig. 7. Estimation results of simulations with time-varying model under noises corrupted measurements: (a)–(d) by FRLS-EKF; (e)–(h) by FBCRLSOE-EKF; (i)–(l) by FBCRLSIE-EKF; (m)–(p) by FBCRLSEIV-EKF.

Table 18. In experiments, similarly to previous simulations, the noises imposed on the battery voltage and current measurements also generate model identification biases and increase SOC estimation error when FRLS-EKF is used. In the experiment with no additional noise (Experiment 1), the estimation results are the closest to the reference values. Due to the model error and the calculation error of the algorithm, the RMSEs of the SOC and the parameters are greater in experiments than that in previous simulations. In the experiment with only additional noise on voltage measurement (Experiment 2), compared with the no additional noise experiment (Experiment 1), the RMSEs of R_1 and φ_1 increase from 28.34 mΩ to 36.66 mΩ and from 0.0216 to 0.0338, but the estimation of R_0 biases slightly and still fluctuates around the reference value. The RMSE of the SOC increases from 1.9615% to 2.3430%. In the experiment with only additional noise on current measurement (Experiment 3), the RMSEs of R_0, R_1 and φ_1 increase to 1.5490 mΩ, 37.11 mΩ and 0.0395, respectively; the RMSE of the SOC increases to 2.4718%. In the experiment with additional noises on both voltage and current measurements (Experiment 4), the RMSEs of R_0, R_1 and φ_1 increase to 1.6237 mΩ, 40.99 mΩ and 0.0543, respectively; and the RMSE of SOC increases to 2.6549%. These results verify that, when FRLS-EKF is used, the noises imposed on battery voltage and current measurements will generate model identification biases and increase SOC estimation errors in not only the EIV problem, but also the OE and the IE

Table 17
Variances of noises imposed on battery voltage and current measurements in experiments.

Experiment No.	Problem type	Variances of noises
Experiment 1	noise free	$\sigma_V^2 = 0\text{mV}^2, \sigma_I^2 = 0\text{A}^2$
Experiment 2	OE	$\sigma_V^2 = 10\text{mV}^2, \sigma_I^2 = 0\text{A}^2$
Experiment 3	IE	$\sigma_V^2 = 0\text{mV}^2, \sigma_I^2 = 0.01\text{A}^2$
Experiment 4	EIV	$\sigma_V^2 = 10\text{mV}^2, \sigma_I^2 = 0.01\text{A}^2$

Table 16
RMSEs of estimation by four kinds of RLS-based-EKF in simulations.

Model type		Time-invariant				Time-varying			
Simulation NO.		1	2	3	4	5	6	7	8
Problem type		noise free	OE	IE	EIV	noise free	OE	IE	EIV
Voltage noise variance (mV^2)		0	10	0	10	0	10	0	10
Current noise variance (A^2)		0	0	0.01	0.01	0	0	0.01	0.01
FRLS-EKF	RMSE of SOC (%)	0.0072	1.1298	1.2417	1.6809	0.1075	1.2824	1.3486	1.8153
	RMSE of R_0 (mΩ)	0.0035	0.3397	2.0111	1.9512	0.2907	0.4131	2.1536	1.8788
	RMSE of R_1 (mΩ)	0.40	27.38	28.96	38.01	4.10	30.89	31.60	41.27
	RMSE of φ_1	0.00013	0.00708	0.00872	0.01859	0.00157	0.00885	0.01062	0.01997
FBCRLSOE-EKF	RMSE of SOC (%)	0.0072	0.0104	0.1746	0.1416	0.1046	0.1153	0.2299	0.2441
	RMSE of R_0 (mΩ)	0.0035	0.3355	2.0445	2.0169	0.2906	0.4090	2.1915	1.9528
	RMSE of	0.39	3.02	5.54	6.02	4.07	5.31	7.89	15.46
	RMSE of φ_1	0.00013	0.00054	0.00102	0.00136	0.00156	0.00173	0.00197	0.00202
FBCRLSIE-EKF	RMSE of SOC (%)	0.0072	0.2006	0.0500	0.2691	0.1044	0.1303	0.0490	0.1607
	RMSE of R_0 (mΩ)	0.0037	2.0565	0.4248	2.3170	0.2938	2.0141	0.5319	2.3378
	RMSE of R_1 (mΩ)	0.39	7.83	3.75	15.73	4.07	8.57	5.41	28.28
	RMSE of φ_1	0.00013	0.00085	0.00053	0.00113	0.00156	0.00229	0.00166	0.00238
FBCRLSEIV-EKF	RMSE of SOC (%)	0.0305	0.0263	0.0250	0.0525	0.0778	0.1136	0.0351	0.0873
	RMSE of R_0 (mΩ)	0.1626	0.6209	0.7094	1.1798	0.3502	0.8348	0.7911	1.1561
	RMSE of R_1 (mΩ)	0.63	3.56	4.03	6.76	3.91	6.01	6.26	8.32
	RMSE of φ_1	0.00005	0.00050	0.00056	0.00080	0.00154	0.00244	0.00182	0.00256

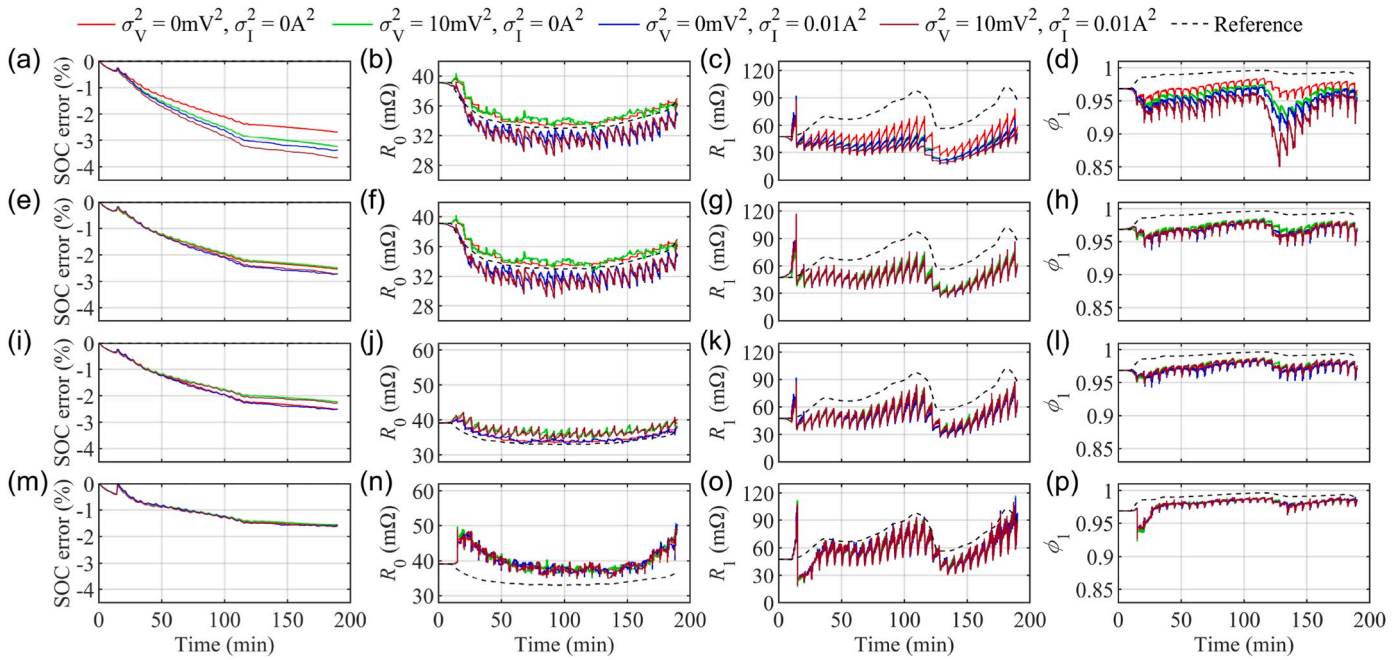

Fig. 8. Estimation results of experiments under noises corrupted measurements: (a)–(d) by FRLS-EKF; (e)–(h) by FBCRLSOE-EKF; (i)–(l) by FBCRLSIE-EKF; (m)–(p) by FBCRLSEIV-EKF.

problems.

The estimation results by FBCRLSOE-EKF are shown in Fig. 8 (e)–(h) and Table 18. In the experiment with only additional noise on voltage measurement (Experiments 2), even though the voltage measurement is corrupted by noise, the RMSEs of the SOC and the parameters increase very slightly and much less than the RMSEs of the estimations by FRLS-EKF. It verifies that, in experiment, the FBCRLSOE-EKF can also compensate the model identification biases and SOC estimation error caused by the noises imposed on voltage measurement. In Experiment 3 and Experiment 4, due to the addition of noise on current measurements, the RMSEs of SOC and parameters estimated by FBCRLSOE-EKF are slightly larger than those in Experiment 2.

The estimation results by FBCRLSIE-EKF are shown in Fig. 8 (i)–(l) and Table 18. In the experiment with only additional noise on current measurement (Experiment 3), even though the current measurement is corrupted by noise, the RMSEs of the SOC and the parameters increase very slightly and much less than the RMSEs of the estimations by FRLS-EKF. It verifies that, in experiment, the FBCRLSIE-EKF can also compensate the model identification biases and SOC estimation error caused by noises imposed on current measurement. In Experiment 2 and Experiment 4, the RMSEs of SOC, R_1 and φ_1 estimated by FBCRLSIE-EKF are slightly lower than those in experiment 3, because, similarly with the trends in simulations, the biases of the estimations are toward to positive direction, which coincidently offset the estimation error caused by the model error.

The estimation results by FBCRLSEIV-EKF are shown in Fig. 8 (m)–(p) and Table 18. The noises, imposed either on one of voltage and current measurements or on both of them, have little influence on the estimation results. It verifies that FBCRLSEIV-EKF can compensate the model identification biases caused by noises imposed on voltage and current measurements. As seen in Table 18, the RMSE of the SOC estimated by FBCRLSEIV-EKF are 1.4526%, 1.4712%, 1.4596% and 1.3937% in Experiment 1 to Experiment 4, respectively, these are less than that by other three co-estimate algorithms. The RMSE of R_1 estimated by FBCRLSEIV-EKF is also less than that by other three co-estimate algorithms. But it is notable that the RMSE of R_0 estimated by FBCRLSEIV-EKF are larger than that by other three co-estimate algorithms in experiments. This may be caused by the modeling error of the battery model. But the R_0 estimated by FBCRLSEIV-EKF are similar in different noises corruption cases, because the biases caused by noises can be compensated by FBCRLSEIV. These results verify that FBCRLSEIV-EKF can compensate the model identification biases and the SOC estimation error caused by noises imposed both on voltage and current measurements.

In summary, in experiments, similarly to the previous simulations, the noises imposed on voltage and current measurements would result in biases in battery model identification and increase the SOC estimation error, when conventional FRLS-EKF is used. The FBCRLSOE-EKF can effectively compensate the model identification biases and the SOC estimation error caused by noises, when only voltage measurement is corrupted by noise; the FBCRLSIE-EKF can effectively compensate the model identification biases and SOC estimation error caused by noises, when only current measurement is corrupted by noise; the FBCRLSEIV-EKF can effectively compensate the model identification biases and SOC estimation error caused by the noises imposed on both voltage and current measurements.

7. Conclusions

The consistent results from formulas and simulations both adequately and quantitatively reveals that the battery model identified by conventional RLS is biased when either only one of voltage and current measurements or both of them are corrupted by white noises. Simulation and experiment studies suggest that the noises imposed on measurements not only result in model identification biases but also greatly degrade the accuracy of SOC estimation, when conventional FRLS-EKF is used.

Then, three joint bias compensation RLS and EKF co-estimation algorithms are proposed to address the adverse noise effect on SOC and parameter estimation for different noise corruption problems. Simulation and experiment studies suggest that, comparing with conventional FRLS-EKF, the proposed bias compensation RLS based co-estimation algorithms can effectively compensate the model identification biases caused by noises and can enhance SOC estimation accuracy in different noise corruption problems. In these algorithms, the FBCRLSOE-EKF is effective when only voltage measurement is corrupted by noise; the

Table 18
RMSEs of estimation by four kinds of RLS-based-EKF in experiments.

Experiment NO.		1	2	3	4
Problem type		noise free	OE	IE	EIV
Voltage noise variance (mV^2)		0	10	0	10
Current noise variance (A^2)		0	0	0.01	0.01
FRLS-EKF	RMSE of SOC (%)	1.9615	2.3430	2.4718	2.6549
	RMSE of R_0(mΩ)	0.7468	0.9593	1.5490	1.6237
	RMSE of R_1(mΩ)	28.34	36.66	37.11	40.99
	RMSE of φ_1	0.0216	0.0338	0.0395	0.0543
FBCRLSOE-EKF	RMSE of SOC (%)	1.8471	1.8169	1.9954	1.9559
	RMSE ofR_0(mΩ)	0.7379	0.9226	1.6044	1.7291
	RMSE of R_1(mΩ)	26.39	26.05	28.10	27.83
	RMSE of φ_1	0.0195	0.0193	0.0230	0.0226
FBCRLSIE-EKF	RMSE of SOC (%)	1.8323	1.6499	1.8635	1.6878
	RMSE of R_0(mΩ)	1.0624	3.0408	1.0992	2.8130
	RMSE of R_1(mΩ)	26.18	23.57	26.40	24.17
	RMSE of φ_1	0.0192	0.0164	0.0197	0.0168
FBCRLSEIV-EKF	RMSE of SOC (%)	1.1891	1.1748	1.2141	1.2217
	RMSE of R_0(mΩ)	6.0741	6.3041	6.1354	6.2135
	RMSE of R_1(mΩ)	18.39	18.25	18.45	18.70
	RMSE of φ_1	0.0138	0.0142	0.0139	0.0140

FBCRLSIE-EKF is effective when only current measurement is corrupted by noise; the FBCRLSEIV-EKF is effective when either only one of voltage and current measurements or both of them are corrupted by noises.

Moreover, the feasibility of the proposed algorithms in online application is evaluated by counting the arithmetic operation requirements of these algorithms. The total number of arithmetic operations for one iteration of FBCRLSOE-EKF, FBCRLSOE-EKF and FBCRLSEIV-EKF are 1.34, 1.34 and 2.40 times of that of FRLS-EKF. Compared with FRLS-EKF, the computation cost of FBCRLSOE-EKF and FBCRLSIE-EKF increase slightly, and that of FBCRLSEIV-EKF increases more, but still not dramatically. It shows that the proposed bias compensation RLS based co-estimation algorithms can be used in online application with moderate growth in computation cost.

Declaration of competing interest

The authors declare that they have no known competing financial interests or personal relationships that could have appeared to influence the work reported in this paper.

Acknowledgements

This work was supported by National Key R&D Program of China (2018YFB0104100).

References

[1] R. Xiong, J. Cao, Q. Yu, H. He, F. Sun, Critical review on the battery state of charge estimation methods for electric vehicles, IEEE Access 6 (2018) 1832–1843, https://doi.org/10.1109/ACCESS.2017.2780258.
[2] R. Xiong, J. Tian, H. Mu, C. Wang, A systematic model-based degradation behavior recognition and health monitoring method for lithium-ion batteries, Appl. Energy 207 (2017) 372–383, https://doi.org/10.1016/j.apenergy.2017.05.124.
[3] X. Hu, F. Sun, Y. Zou, Comparison between two model-based algorithms for Li-ion battery SOC estimation in electric vehicles, Simulat. Model. Pract. Theor. 34 (2013) 1–11, https://doi.org/10.1016/j.simpat.2013.01.001.
[4] S. Rodrigues, N. Munichandraiah, A.K. Shukla, A review of state-of-charge indication of batteries by means of a.c. impedance measurements, J. Power Sources 87 (2000) 12–20, https://doi.org/10.1016/S0378-7753(99)00351-1.
[5] H. Sheng, J. Xiao, Electric vehicle state of charge estimation: nonlinear correlation and fuzzy support vector machine, J. Power Sources 281 (2015) 131–137, https://doi.org/10.1016/j.jpowsour.2015.01.145.
[6] E. Walker, S. Rayman, R.E. White, Comparison of a particle filter and other state estimation methods for prognostics of lithium-ion batteries, J. Power Sources 287 (2015) 1–12, https://doi.org/10.1016/j.jpowsour.2015.04.020.
[7] L. Kang, X. Zhao, J. Ma, A new neural network model for the state-of-charge estimation in the battery degradation process, Appl. Energy 121 (2014) 20–27, https://doi.org/10.1016/j.apenergy.2014.01.066.
[8] T. Weigert, Q. Tian, K. Lian, State-of-charge prediction of batteries and battery-supercapacitor hybrids using artificial neural networks, J. Power Sources 196 (2011) 4061–4066, https://doi.org/10.1016/j.jpowsour.2010.10.075.
[9] W. He, N. Williard, M. Osterman, M. Pecht, Prognostics of lithium-ion batteries based on Dempster–Shafer theory and the Bayesian Monte Carlo method, J. Power Sources 196 (2011) 10314–10321, https://doi.org/10.1016/j.jpowsour.2011.08.040.
[10] Y. Shen, Adaptive online state-of-charge determination based on neuro-controller and neural network, Energy Convers. Manag. 51 (2010) 1093–1098, https://doi.org/10.1016/j.enconman.2009.12.015.
[11] Q. Yu, R. Xiong, C. Lin, W. Shen, J. Deng, Lithium-ion battery parameters and state-of-charge joint estimation based on H-infinity and unscented Kalman filters, IEEE Trans. Veh. Technol. 66 (2017) 8693–8701, https://doi.org/10.1109/TVT.2017.2709326.
[12] Y. Wang, C. Zhang, Z. Chen, A method for state-of-charge estimation of Li-ion batteries based on multi-model switching strategy, Appl. Energy 137 (2015) 427–434, https://doi.org/10.1016/j.apenergy.2014.10.034.
[13] S. Sepasi, R. Ghorbani, B.Y. Liaw, Improved extended Kalman filter for state of charge estimation of battery pack, J. Power Sources 255 (2014) 368–376, https://doi.org/10.1016/j.jpowsour.2013.12.093.
[14] H. Dai, X. Wei, Z. Sun, J. Wang, W. Gu, Online cell SOC estimation of Li-ion battery packs using a dual time-scale Kalman filtering for EV applications, Appl. Energy 95 (2012) 227–237, https://doi.org/10.1016/j.apenergy.2012.02.044.
[15] G. Perez, M. Garmendia, J. Francois Reynaud, J. Crego, U. Viscarret, Enhanced closed loop State of Charge estimator for lithium-ion batteries based on Extended Kalman Filter, Appl. Energy 155 (2015) 834–845, https://doi.org/10.1016/j.apenergy.2015.06.063.
[16] G.L. Plett, Extended Kalman filtering for battery management systems of LiPB-based HEV battery packs Part 3. State and parameter estimation, J. Power Sources 134 (2004) 277–292, https://doi.org/10.1016/j.jpowsour.2004.02.033.
[17] B. Xia, H. Wang, M. Wang, W. Sun, Z. Xu, Y. Lai, A new method for state of charge estimation of lithium-ion battery based on strong tracking Cubature Kalman filter, Energies 8 (2015) 13458–13472, https://doi.org/10.3390/en81212378.
[18] S.K. Rahimian, S. Rayman, R.E. White, State of charge and loss of active material estimation of a lithium ion cell under low earth orbit condition using Kalman filtering approaches, J. Electrochem. Soc. 159 (2012) A860–A872, https://doi.org/10.1149/2.098206jes.
[19] S. Santhanagopalan, R.E. White, Online estimation of the state of charge of a lithium ion cell, J. Power Sources 161 (2006) 1346–1355, https://doi.org/10.1016/j.jpowsour.2006.04.146.
[20] B. Xiong, J. Zhao, Z. Wei, M. Skyllas-Kazacos, Extended Kalman filter method for state of charge estimation of vanadium redox flow battery using thermal-dependent electrical model, J. Power Sources 262 (2014) 50–61, https://doi.org/10.1016/j.jpowsour.2014.03.110.
[21] Y. Wang, C. Zhang, Z. Chen, A method for state-of-charge estimation of LiFePO 4 batteries at dynamic currents and temperatures using particle filter, J. Power Sources 279 (2015) 306–311, https://doi.org/10.1016/j.jpowsour.2015.01.005.
[22] M. Ye, H. Guo, B. Cao, A model-based adaptive state of charge estimator for a lithium-ion battery using an improved adaptive particle filter, Appl. Energy 190 (2017) 740–748, https://doi.org/10.1016/j.apenergy.2016.12.133.
[23] Y. Wang, C. Zhang, Z. Chen, On-line battery state-of-charge estimation based on an integrated estimator, Appl. Energy 185 (2017) 2026–2032, https://doi.org/10.1016/j.apenergy.2015.09.015.
[24] X. Hu, F. Sun, Y. Zou, Estimation of state of charge of a lithium-ion battery pack for electric vehicles using an adaptive luenberger observer, Energies 3 (2010) 1586–1603, https://doi.org/10.3390/en3091586.
[25] Q. Zhu, L. Li, X. Hu, N. Xiong, G. Hu, H∞-Based nonlinear observer design for state of charge estimation of lithium-ion battery with polynomial parameters, IEEE Trans. Veh. Technol. 66 (2017) 10853–10865, https://doi.org/10.1109/TVT.2017.2723522.
[26] Q. Zhu, N. Xiong, M. Yang, R. Huang, G. Hu, State of charge estimation for lithium-ion battery based on nonlinear observer: an H∞ method, Energies 10 (2017) 679, https://doi.org/10.3390/en10050679.
[27] C. Lin, H. Mu, R. Xiong, W. Shen, A novel multi-model probability battery state of charge estimation approach for electric vehicles using H-infinity algorithm, Appl. Energy 166 (2016) 76–83, https://doi.org/10.1016/j.apenergy.2016.01.010.
[28] X. Chen, W. Shen, Z. Cao, A. Kapoor, A novel approach for state of charge estimation based on adaptive switching gain sliding mode observer in electric vehicles, J. Power Sources 246 (2014) 667–678, https://doi.org/10.1016/j.jpowsour.2013.08.039.
[29] F. Zhong, H. Li, S. Zhong, Q. Zhong, C. Yin, An SOC estimation approach based on adaptive sliding mode observer and fractional order equivalent circuit model for lithium-ion batteries, Commun. Nonlinear Sci. 24 (2015) 127–144, https://doi.org/10.1016/j.cnsns.2014.12.015.
[30] Z. Wei, S. Meng, B. Xiong, D. Ji, K.J. Tseng, Enhanced online model identification and state of charge estimation for lithium-ion battery with a FBCRLS based observer, Appl. Energy 181 (2016) 332–341, https://doi.org/10.1016/j.apenergy.2016.08.103.

[31] W. Waag, C. Fleischer, D.U. Sauer, Critical review of the methods for monitoring of lithium-ion batteries in electric and hybrid vehicles, J. Power Sources 258 (2014) 321–339, https://doi.org/10.1016/j.jpowsour.2014.02.064.
[32] F. Liu, F. Lan, J. Chen, Dynamic thermal characteristics of heat pipe via segmented thermal resistance model for electric vehicle battery cooling, J. Power Sources 321 (2016) 57–70, https://doi.org/10.1016/j.jpowsour.2016.04.108.
[33] W. Waag, C. Fleischer, D.U. Sauer, Critical review of the methods for monitoring of lithium-ion batteries in electric and hybrid vehicles, J. Power Sources 258 (2014) 321–339, https://doi.org/10.1016/j.jpowsour.2014.02.064.
[34] H. He, R. Xiong, H. Guo, Online estimation of model parameters and state-of-charge of LiFePO4 batteries in electric vehicles, Appl. Energy 89 (2012) 413–420, https://doi.org/10.1016/j.apenergy.2011.08.005.
[35] G.L. Plett, Sigma-point Kalman filtering for battery management systems of LiPB-based HEV battery packs Part 2: simultaneous state and parameter estimation, J. Power Sources 161 (2006) 1369–1384, https://doi.org/10.1016/j.jpowsour.2006.06.004.
[36] F. Zhang, G. Liu, L. Fang, Battery state estimation using unscented Kalman filter, in: IEEE International Conference on Robotics and Automation. Kobe2009, 2009, pp. 1863–1868, https://doi.org/10.1109/ROBOT.2009.5152745.
[37] G.L. Plett, Sigma-point Kalman filtering for battery management systems of LiPB-based HEV battery packs Part 1: introduction and state estimation, J. Power Sources 161 (2006) 1356–1368, https://doi.org/10.1016/j.jpowsour.2006.06.003.
[38] R. Xiong, F. Sun, Z. Chen, H. He, A data-driven multi-scale extended Kalman filtering based parameter and state estimation approach of lithium-ion olymer battery in electric vehicles, Appl. Energy 113 (2014) 463–476, https://doi.org/10.1016/j.apenergy.2013.07.061.
[39] C. Hu, B.D. Youn, J. Chung, A multiscale framework with extended Kalman filter for lithium-ion battery SOC and capacity estimation, Appl. Energy 92 (2012) 694–704, https://doi.org/10.1016/j.apenergy.2011.08.002.
[40] R. Xiong, F. Sun, X. Gong, C. Gao, A data-driven based adaptive state of charge estimator of lithium-ion polymer battery used in electric vehicles, Appl. Energy 113 (2014) 1421–1433, https://doi.org/10.1016/j.apenergy.2013.09.006.
[41] X. Guo, L. Kang, Y. Yao, Z. Huang, W. Li, Joint estimation of the electric vehicle power battery state of charge based on the least squares method and the Kalman filter algorithm, Energies 9 (2016) 100, https://doi.org/10.3390/en9020100.
[42] Y. Li, C. Wang, J. Gong, A combination Kalman filter approach for State of Charge estimation of lithium-ion battery considering model uncertainty, Energy 109 (2016) 933–946, https://doi.org/10.1016/j.energy.2016.05.047.
[43] H. Rahimi-Eichi, F. Baronti, M. Chow, Online adaptive parameter identification and state-of-charge coestimation for lithium-polymer battery cells, IEEE Trans. Ind. Electron. 61 (2014) 2053–2061, https://doi.org/10.1109/TIE.2013.2263774.
[44] B. Xia, Z. Lao, R. Zhang, Y. Tian, G. Chen, Z. Sun, et al., Online parameter identification and state of charge estimation of lithium-ion batteries based on forgetting factor recursive least squares and nonlinear Kalman filter, Energies 11 (2018) 3, https://doi.org/10.3390/en11010003.
[45] Z. Lao, B. Xia, W. Wang, W. Sun, Y. Lai, M. Wang, A novel method for lithium-ion battery online parameter identification based on variable forgetting factor recursive least squares, Energies 11 (2018) 1358, https://doi.org/10.3390/en11061358.
[46] T. Söderström, Errors-in-variables methods in system identification, Automatica 43 (2007) 939–958, https://doi.org/10.1016/j.automatica.2006.11.025.
[47] J.G. Linden, T. Larkowski, K.J. Burnham, Algorithms for recursive/semi-recursive bias-compensating least squares system identification within the errors-in-variables framework, Int. J. Contr. 85 (2012) 1625–1643, https://doi.org/10.1080/00207179.2012.696145.
[48] W.X. Zheng, Transfer function estimation from noisy input and output data, Int. J. Adapt. Contr. 12 (1998) 365–380, https://doi.org/10.1002/(SICI)1099-1115(199806)12:4<365::AID-ACS496>3.0.CO;2-A.
[49] M.U. Cuma, T. Koroglu, A comprehensive review on estimation strategies used in hybrid and battery electric vehicles, Renew. Sustain. Energy Rev. 42 (2015) 517–531, https://doi.org/10.1016/j.rser.2014.10.047.
[50] M. Sitterly, L.Y. Wang, G.G. Yin, C. Wang, Enhanced identification of battery models for real-time battery management, IEEE Trans. Sustain. Energy 2 (2011) 300–308, https://doi.org/10.1109/TSTE.2011.2116813.
[51] L. Liu, L.Y. Wang, Z. Chen, C. Wang, F. Lin, H. Wang, Integrated system identification and state-of-charge estimation of battery systems, IEEE Trans. Energy Convers. 28 (2013) 12–23, https://doi.org/10.1109/TEC.2012.2223700.
[52] Z. Wei, C. Zou, F. Leng, B.H. Soong, K. Tseng, Online model identification and state-of-charge estimate for lithium-ion battery with a recursive total least squares-based observer, IEEE Trans. Ind. Electron. 65 (2018) 1336–1346, https://doi.org/10.1109/TIE.2017.2736480.
[53] Z. Wei, J. Zhao, C. Zou, T.M. Lim, K.J. Tseng, Comparative study of methods for integrated model identification and state of charge estimation of lithium-ion battery, J. Power Sources 402 (2018) 189–197, https://doi.org/10.1016/j.jpowsour.2018.09.034.
[54] A.G. Wu, S. Chen, D.L. Jia, Bias-compensation-based least-squares estimation with a forgetting factor for output error models with white noise, Int. J. Syst. Sci. 47 (2016) 1700–1709, https://doi.org/10.1080/00207721.2014.948945.
[55] X. Lai, Y. Zheng, T. Sun, A comparative study of different equivalent circuit models for estimating state-of-charge of lithium-ion batteries, Electrochim. Acta 259 (2018) 566–577, https://doi.org/10.1016/j.electacta.2017.10.153.
[56] H. He, R. Xiong, H. Guo, S. Li, Comparison study on the battery models used for the energy management of batteries in electric vehicles, Energy Convers. Manag. 64 (2012) 113–121, https://doi.org/10.1016/j.enconman.2012.04.014.
[57] X. Hu, S. Li, H. Peng, A comparative study of equivalent circuit models for Li-ion batteries, J. Power Sources 198 (2012) 359–367, https://doi.org/10.1016/j.jpowsour.2011.10.013.
[58] H. He, R. Xiong, J. Fan, Evaluation of lithium-ion battery equivalent circuit models for state of charge estimation by an experimental approach, Energies 4 (2011) 582–598, https://doi.org/10.3390/en4040582.
[59] F. Zheng, Y. Xing, J. Jiang, B. Sun, J. Kim, M. Pecht, Influence of different open circuit voltage tests on state of charge online estimation for lithium-ion batteries, Appl. Energy 183 (2016) 513–525, https://doi.org/10.1016/j.apenergy.2016.09.010.
[60] L. Ljung, System Identification: Theory for the User, second ed., Prentice Hall, 1999.
[61] Z. Wei, T.M. Lim, M. Skyllas-Kazacos, N. Wai, K.J. Tseng, Online state of charge and model parameter co-estimation based on a novel multi-timescale estimator for vanadium redox flow battery, Appl. Energy 172 (2016) 169–179, https://doi.org/10.1016/j.apenergy.2016.03.103.
[62] R. Xiong, F. Sun, H. He, T.D. Nguyen, A data-driven adaptive state of charge and power capability joint estimator of lithium-ion polymer battery used in electric vehicles, Energy 63 (2013) 295–308, https://doi.org/10.1016/j.energy.2013.10.027.